An Elastic Second Skin

Betty Yu[1], Soo-Young Kang[1], Ariya Akthakul[2], Nithin Ramadurai[2], Morgan Pilkenton[1], Alpesh Patel[1], Amir Nashat[2], Daniel G. Anderson[3,4,5,6], Fernanda H. Sakamoto[7], Barbara A. Gilchrest[8], R. Rox Anderson[7] and Robert Langer[3,4,5,6*]

[1] Living Proof, Inc., Cambridge, MA 02142, USA
[2] Olivo Laboratories, LLC., Cambridge, MA 02142 USA
[3] Institute for Medical Engineering and Science, Massachusetts Institute of Technology, Cambridge, MA, 02139, USA
[4] Harvard-MIT Division of Health Science and Technology, Massachusetts Institute of Technology, Cambridge, MA, 02139, USA
[5] David H. Koch Institute for Integrative Cancer Research, Massachusetts Institute of Technology, Cambridge, MA, 02139, USA
[6] Department of Chemical Engineering, Massachusetts Institute of Technology, Cambridge, MA 02139, USA
[7] The Wellman Center for Photomedicine, Massachusetts General Hospital and Harvard Medical School, Boston, MA 02114, USA
[8] Department of Dermatology, Massachusetts General Hospital and Harvard Medical School, Boston, MA 02114, USA

*To whom correspondence should be addressed.

ABSTRACT

We report the synthesis and application of an elastic, wearable crosslinked polymer layer (XPL) that mimics the properties of normal, youthful skin. XPL is made of a tunable polysiloxane-based material that can be engineered with specific elasticity, contractility, adhesion, tensile strength and occlusivity. XPL can be topically applied, rapidly curing at the skin interface without the need for heat- or light-mediated activation. In a pilot human study, we examined the performance of a prototype XPL that has a tensile modulus matching normal skin responses at low strain (< 40%), and that withstands elongations exceeding 250%, elastically recoiling with minimal strain-energy loss on repeated deformation. The application of XPL to the herniated lower-eyelid fat pads of 12 subjects resulted in an average 2-grade decrease in herniation appearance in a 5-point severity scale. The XPL platform may offer advanced solutions to compromised skin barrier function, pharmaceutical delivery, and wound dressings.

INTRODUCTION

The skin is a versatile organ with multiple physiological functions, performed in the context of a fluctuating environment. Importantly, the skin is a visible organ and, thus, makes a psychosocial

statement about the health of the individual. The primary function of skin is to provide a protective barrier that mitigates exposure to external factors such as extreme temperatures, toxins, microorganisms, radiation, and mechanical insult, while maintaining the internal milieu.

The important role of skin is inevitably compromised by aging, environmental insult, and certain disease states. Conditions characterized by skin barrier dysfunction remain prevalent in the population[1,2,3,4]. Cutaneous water loss is clinically observed as chronic inflammation and pruritus that are, in turn, responsible for decreased quality of life, deranged sleep patterns, and mood disturbances that include anxiety and depression[5]. Skin aging, whether chronological or accelerated by sun exposure, creates persistent problems that will be faced by all members of society[6]. As the skin ages, it loses biomechanical integrity, while also becoming more susceptible to environmental injury[6] and impaired wound healing[7].

The aging-related changes in skin mechanical integrity result primarily in loss of elastic recoil and baseline laxity. This loss of elastic recoil is not reversible by existing therapies[8] and consequently remains the universal fate of our largest and most visible organ[9]. Recent progress in materials science and engineering have yielded flexible skin interfacing technologies[10,11,12] that are functionalized in some cases for pharmaceutical delivery[13], rapid analyte detection[14], continuous physiological monitoring of medical conditions[15], and wound healing[16,17,18]. Unfortunately, these advances have not focused on restoring the mechanical and aesthetic properties of the skin to match its original, youthful state.

Existing solutions fall short of addressing both the mechanical and physiological functions of normal healthy skin. Individuals with compromised skin barrier function, for example, still rely on the use of cumbersome occlusive dressings, often in combination with topical ointments that often fail due to poor patient compliance[3]. Although, existing flexible and skin-adherent pre-formed films interface with the skin[15,19,20,21], these materials are not designed to serve as a 'second skin' that can be worn invisibly to restore normal skin recoil and aesthetics.

The design and adoption of such a 'second skin' with respect to a wearable, skin-conformal material via topical application pose several fundamental challenges. First, the material must be safe on skin without irritation and sensitization. Second, the material must be incorporated in a topical formulation that is readily spreadable on skin and form a safe 'second skin' *in-situ*. Third,

the material must adhere to skin, while providing a breathable, but protective, interface to the environment. Fourth, the material must possess mechanical properties that accommodate normal skin mechanical responses to motion while reinforcing inherent skin tension and elastic recoil. Fifth, the material must mimic, or at least not interfere with, the appearance of healthy normal skin, for a wide range of individual skin types.

Based on the above design challenges, we selected the XPL chemistry for siloxane polymers and their associated cross-linked networks in part as a result of the numerous safety and biocompatibility data existing in the literature[22,23]. In addition to the established safety profile, silicone cross-linked networks offer readily tunable architectures that enable the development of materials which are optimizable for a myriad target mechanical and transport properties, such as flexibility, elongation, elasticity, toughness, adhesion, and moisture/oxygen permeability. The room-temperature, platinum-catalyzed hydrosilylation chemistry we selected does not yield reaction by-products which are typical of condensation reactions, nor is it dependent on additional energy sources, such as heat or UV, required to initiate the topical cross-linking reaction *in-situ*. Therefore, the XPL can be safely and easily deposited on skin *in-situ* via a two-step topical delivery system, where the first step comprises the application of a flowable, skin-conformal, reactive polysiloxane film which is then cross-linked upon exposure to the platinum catalyst that is introduced in the second step. The two-step system also enables optical modulation of the second skin by depositing light scattering particles at the XPL surface via the second step delivery vehicle. The complement of the surface optical particles and the underlying cross-linked polysiloxane network generates a specular and diffuse reflectance approximating the appearance of youthful skin.

In essence, the XPL presented in this study is a skin-adherent, three-dimensional polymer network that is chemically cross-linked in situ on skin, following a two-step topical application process. Each of the materials selected in the formulations is either on the US Food and Drug Administrations (FDA) list of Generally Regarded as Safe (GRAS) substances, or has individual safety documents that demonstrate safety for leave-on skin applications. Here, we report the design and development of a biomimetic skin-conforming cross-linked polymer material that can be formulated for easy topical application to form an “invisible” elastic film *in-situ*. The film can

be safely worn on the skin, restores normal skin aesthetics, and exerts stresses in the plane of the skin to change its form. The tunability of the cross-linked polymer layer (XPL) chemistry and its corresponding ingredients in the topical formulation render this 'second skin' platform potentially useful for a wide range of cosmetic and medical applications.

RESULTS

Material Synthesis for Network Architecture that Optimizes Elastic Response

Uniaxial tensile testing that investigated skin anisotropy with respect to the Langer Lines (topological lines corresponding to structural orientation of collagen fibers in the dermis) at different body locations and orientations reported a linear elastic deformation zone at low strains (up to 10% to 40%) and corresponding elastic moduli ranging from 0.5 MPa to 1.95 MPa, with the resulting fracture strain measured at 140% to 180%[24]. Based on these established skin mechanical properties, the target XPL modulus space was identified at 0.5 MPa to 1.95 MPa, and the elastic strain region was specified to be greater than 180%.

To identify polymer compositions exhibiting the target design criteria, a material library was generated by systematically varying the following parameters: (1) relative functional (vinyl- and hydride-) polysiloxane chain lengths, (2) the cross-link density as a function of the corresponding functional polysiloxane concentrations, and (3) the concentration of reinforcing fumed silica. A plot of the fracture strain as a function of the tensile modulus illustrates the mechanical design space spanned by the materials synthesized from the screen (See Figure 7 of the Supplementary Information), where over 100 reactive polymer blend compositions (RPB) yielded tensile moduli ranging from 0.1 MPa to 2.5 MPa and fracture strains as high as 800%. Based on an analysis of reported values, we restricted our analysis of the library to formulations with tensile moduli between 0.4 and 0.8 MPa. A lead RPB candidate, with tensile modulus of 0.48 MPa, fracture strain of 826%, and adhesive strength of 78 N/mm, that also satisfied the elasticity criteria (plastic strain of 1.3% and hysteresis strain energy density loss of 0.66 kJ/m^3 following cyclic loading at 15% strain), was selected based on an optimization of the material performance attributes desired for a biomimetic 'second skin' (see Table 1 in Supplementary Information). This lead RPB was later incorporated with other excipients into the final two-step delivery system to form the XPL *in-situ*.

Although the fumed silica imparts mechanical toughness to the XPL films, it also exponentially increased the viscosity of the RPB. As a result, the lead RPB (containing 27% w/w fumed silica) demonstrated poor topical spreading properties, with a viscosity of 600 Pa.s (600,000 cP) measured at 0.5 sec^{-1}. At such a high viscosity, the RPB spreadability on skin approximated that of the tar pitch. The detailed formulation strategies of this material are discussed in Methods.

Mechanical Properties of the XPL

Three key mechanical design criteria in the development of the skin mimetic XPL required that the elastic recoil, flexibility, and elongation approximated the values of natural skin subjected to an initial elastic large deformation zone (strain under 40% and tensile modulus of 0.5-1.95 MPa)[25,26]. In Figure 1a, we report that the XPL maintained elastic recoil until break (fracture strain: 250 ± 82%) and the tensile modulus (0.51 ± 0.01 MPa) measured was comparable to that of natural skin. The measure of elastic recoil (elasticity) was based on the energy loss during the load-unload cycles of the material, quantifiable via the area under the hysteresis loop of the stress-strain profile during tensile testing (hysteresis strain energy density loss). The measured XPL elasticity was 16.8 ± 0.8 kJ/m^3 of hysteresis strain energy density loss with less than 1% plastic strain, following 25 load-unload cycles at 100% strain. We tested elasticity at 100% strain to capture a conservative safety factor of material performance that stretches beyond the reported elastic region for normal skin (less than 40% strain).

With the above mechanical properties to match those of natural skin, we compared the XPL as a wearable skin-conforming material with example commercial benchmarks of film wear on skin, either through pre-formed wound dressings or topical film former formulations.

First, the XPL was compared with two commercial benchmarks of pre-formed wound dressings: Cica-Care® silicone gel sheets (Smith and Nephew, Victoria, Andover, MA) and Tegaderm™ polyurethane sheets coated with acrylic adhesive (3M, St. Paul, Minnesota). As shown in Figure 1a, similar to the XPL, pre-formed Cica-Care® silicone elastomer sheets displayed robust elastic recoil until break (fracture strain: 553 ± 82%), with an order of magnitude lower tensile modulus (0.08 ± 0.04 MPa) compared with that of natural skin (0.5-1.95 MPa). These results confirmed that the topically deposited XPL provides a 3-D silicone network comparable to pre-formed

commercial silicone elastomer sheets, with mechanical properties much closer to those of natural skin.

In contrast to the Cica-Care®, pre-formed Tegaderm™ polyurethane sheets displayed plastic deformation profiles that yield after 15% strain, highlighting an elastic strain region much less than that of natural skin. Moreover, the measured Tegaderm™ tensile modulus of 8.85 ± 2.20 MPa was approximately 7 times greater than natural skin. For comparison, Tegaderm™ displayed substantially greater plastic deformation than XPL following 25 load-unload cycles at 100% strain, as seen by the order of magnitude increases in the hysteresis strain energy density loss and plastic strain measured at 237.0 ± 25.5 kJ/m^3 and 13.56 ± 1.25%, respectively.

Poor elasticity was also measured for the film deposited from the topical film-forming polyurethane dispersion, Avalure™ UR450 (Lubrizol, Wickliffe, OH), a raw material ingredient used in topical personal care products such as make-up, sunscreens, and barrier creams. Avalure™ UR450 demonstrated a tensile modulus that was greater than 30 times that of natural skin (37.6 MPa) and that yielded after 15% strain. Figure 9 (see Supplementary Information) compares the stress-strain hysteresis loops for polyurethane UR450 and the XPL, where polyurethane UR450 yielded with a 12% loss in tensile modulus and plastically deformed with 2% plastic strain, after only 15 load-unload cycles at 15% strain.

In light of the mechanical characteristics displayed by the commercial benchmarks, these results further reinforced the uniqueness of the XPL composition as a topically applied, skin adherent, elastomeric network with mechanical properties optimized to match those of natural skin in motion. Moreover, the XPL demonstrated superior skin cosmesis when compared with the commercial benchmarks. Pre-formed Cica-Care® silicone sheets are 20 times thicker (1,300 microns) and visibly prominent on the skin, resulting from the glossy, light reflective optics that also delineate the film boundary. The 40-micron thick films (Tegaderm™ and polyurethane UR450), which approximated the XPL thickness, were also highly visible on skin as a result of the mismatched film optics, which were further accentuated by the generation of film wrinkling patterns on skin in motion.

In-Vivo Application and Use

This section describes four *in-vivo* studies evaluating the XPL utility as a natural-looking, elastic 'second skin'. Pilot human studies were performed to measure changes in the skin mechanical properties and barrier function after wearing XPL on the lower lids where under-eye fat pads may be prominent (Study A) and on normal volar forearm skin (Study B). To further investigate the XPL as a 'second skin' for conditions of compromised barrier function, transepidermal water loss was measured in clinically dry leg skin (Study C). Finally, the clinical performance of the XPL was evaluated in a double-blind, randomized, placebo-controlled study to demonstrate the translation of the above design criteria (safe, topically-formed *in-situ*, skin-adherent, skin-conforming barrier protection, and natural-looking) to the skin of the lower lid application sites during normal wear (Study D).

Study A: Mechanical Reshaping of the Lower Lid Region

Study A explored the feasibility of reshaping of the lower lid region over time following the application of the XPL and the subsequent progression of the cross-linking reaction *in-situ*. In older individuals, there is often a protrusion of the fat pad underlying the skin in the lower lid area. In this study, a 5-point 0-4 photo-numeric lower lid herniation scale was introduced to quantify the changes in the extent of fat pad herniation following XPL treatment. We hypothesized that the protrusion of the fat pad underlying the skin in the lower lid area could potentially be corrected by a steady, compressive force imparted to the skin by the XPL. Based on our two-step topical delivery system, the compressive force results from the collapse of the polymer coil network during solvent loss, rather than by the chemical bond formation during hydrosilylation. Therefore, in the selection of the lead XPL studied here, the solvents and their concentrations in the formulations were optimally selected to provide sufficient compression-based shrinkage of the skin with minimal discomfort.

As seen in Figure 1b, perceivable reshaping of the lower lid region for a subject with severe bags (severity grade of 4) occurs as the XPL reaction proceeds. To study the cross-linking kinetics of the XPL after the two-step topical delivery system on skin, the relative storage modulus of the XPL was measured *in-vitro* as a function of time, following the introduction of the platinum catalyst, also shown in Figure 1b. The start of the first inflection region of the curve corresponds to the initiation of the cross-linking reaction, which is analogous to the exposure of the Step 1

formulation on skin to the Step 2 formulation comprising 200 ppm platinum catalyst. The steep increase in the normalized storage modulus over approximately 100 seconds provides an indication of how quickly the XPL is generated *in-situ*. The final region of the S-shape curve represents a slower rate of change in the modulus as the reaction asymptotically approaches completion. The delay in the onset of cross-linking indicated at times t<0 was the effect of the catalytic stabilizer introduced in the sample preparation protocol to allow for sufficient working time to conduct experimental measurement. At t=0 seconds, the cross-linking reaction was initiated. The storage modulus approached 80% of the plateau value at t=175 seconds and then levelled off, corresponding to the approach of reaction completion. The photos of the subject shown at baseline, 2 minutes after XPL application, and 3 hours following XPL application depict the immediate impact of the XPL on flaccid skin, followed by the impact on bag compression which occurs over a longer time frame (3 hours to peak). This immediate effect reflects the rapid XPL cross-linking kinetics depicted in Figure 1b, where close to 80% of the final elastic modulus value was achieved over the course of 2 minutes. Notably, the fat pad herniation demonstrated a 2-grade improvement, shown additionally in Figure 2. Such a result has been previously achieved only by a lower lid blepharoplasty, an invasive surgical procedure. Sequential frames extracted from a time-lapse video (Figure 3), demonstrated recovery of skin elasticity after XPL application to lax skin (Figure 3a). The skin was tented (pinched) for 3 seconds with equal pressure on the XPL-treated (right) and XPL-untreated (left) lower lids and then released (Figure 3b). Immediately after the skin was released (Figure 3c), and 3 seconds (Figure 3d) following release, there was a clear difference in the skin recoil between both sides. While the right lower lid (XPL applied) retracted to its original shape, the untreated lid remained tented as a result of the remaining plastic strain from the imposed stress.

Study B: Improved Elastic Recoil of Volar Forearm Skin

Study B explored the mechanical impact of the XPL layer on skin over a 24-hour wear period and after XPL removal, to evaluate the XPL-induced modulation of skin elasticity during wear and the potential residual effects on the underlying internal skin stresses following XPL removal. The clinical changes in skin mechanical properties for six subjects were evaluated at baseline, following 24 hours of XPL wear, and 30 minutes following XPL removal. Using a suction cup

device, the volar arm skin was distended to a fixed position of 12% strain and then released. This test procedure enables the measurement of bulk skin retraction properties, a clinical indicator of skin mechanical function akin to the dermatologic skin tenting test. The negative pressure detected in the suction chamber scales with the skin distensibility, and the retraction times provide an indication of skin elasticity[27,28]. Figure 4a shows a representative skin distensibility plot over 5 consecutive cycles of vacuum application to a representative untreated skin site at baseline. For the first cycle, the elastic and the viscoelastic regions are highlighted by the blue and the red lines, respectively. As expected, under low strains, the skin demonstrates linear elastic behavior, corresponding to the initial linear increase in negative pressure with time; at higher strain, the skin exhibits viscoelastic behavior with a corresponding nonlinear negative pressure dependence on time[29]. Skin hysteresis was also observed over the 5 strain cycles, as characterized by the successive decrease in negative pressure required to induce the fixed strain (Figure 4a).

The skin retraction properties corresponding to XPL treated skin sites following 24 hours of wear demonstrated a consistent, linear response (Figure 4b). Compared to the untreated skin sites at baseline, the consistent linear slope resulting from sequential strain cycles with minimal hysteresis demonstrates the linear elastic behavior exhibited by the bulk skin when the XPL is worn. With the XPL, faster retraction times were also measured along with lower negative pressures required to achieve the target distension height. Thirty-five minutes following XPL removal, the skin distension curve (solid diamonds) approached the baseline value, while not fully displaying the baseline viscoelastic behavior, suggesting a transient skin memory resulting from the prior 24 hours of XPL wear. In summary, the XPL-coated skin exhibited greater elasticity than normal, uncoated skin.

For the six subjects, significant decreases in the average skin retraction time and the average vacuum pressure corresponding to the 12% strain were also measured (36% and 28%, respectively in Figure 4c and Figure 4d), compared to the corresponding baseline values (Figure 4b). Both measurements returned to the baseline values at 35 minutes following XPL removal.

Skin hydration resulting from XPL wear was evaluated in 24 volunteers, aged 22-55, using a skin surface hygrometer to measure skin conductance. The change in skin conductance from baseline

values was calculated for sites treated with the XPL and with the petrolatum at baseline, 1, 2, 4, and 6 hours following test article application (see Figure 4e). Significant increases in skin conductance were measured for the petrolatum and the XPL treated sites ($p<0.05$ and $p<0.001$, respectively). Moreover, the XPL treated sites demonstrated significantly higher increases in conductivity over the six hours of test article wear compared to the petrolatum treated sites ($p<0.05$). The skin hydration properties of the XPL were further complemented by the measurement of transepidermal water loss in subjects with clinically dry skin, described below.

Study C: Improved Transepidermal Water Loss for Dry Skin

Study C explored the XPL aspect as a 'second skin' barrier against transepidermal water loss (TEWL). The XPL barrier effect was measured on the legs of 22 volunteers with moderately to severely dry skin at the test sites, based on a 9-point visual dryness scale. In this study, the XPL was compared with petrolatum, the most effective skin occlusive reported in the literature[30], and a cosmetically elegant, "high end" commercial moisturizer. An untreated control site served as the fourth test site. TEWL values were measured at baseline, 2 hours, and at 24 hours following test article application (Figure 5). Two hours following test article application, the petrolatum and the XPL treated skin sites showed significantly decreased TEWL values relative to the untreated control sites ($p<0.05$ and $p<0.001$, respectively), while the cosmetically elegant moisturizer did not. At 24 hours following test article application, a 23% decrease in the TEWL values from the baseline (-0.95 ± 0.41 g/m^{2}hr, $p<0.01$) persisted at the XPL sites, while there was no decrease in TEWL compared to baseline at the other sites. The results confirmed the XPL as a 'second skin' barrier that protects the skin from excessive moisture loss to the environment.

Study D: Second Skin Performance with Normal Wear

Study D explored the clinical performance of the XPL during normal wear in reshaping the lower lid. Notably, the elastic and adhesive properties of the XPL detailed above are important, as facial expressions invoke repeated stress and strain to the under-eye area, creating a challenge to the XPL 'second skin' durability during normal wear.

To begin characterizing the XPL-induced changes in skin mechanics and cosmesis, two 0-4 photonumeric scales were developed to enable quantification of XPL-induced skin shape changes by trained observers. The potential mechanisms responsible for the observed effects were

further studied using optical coherence tomography (OCT) to non-invasively examine the underlying changes in the hydration and the mechanics of the skin that interfaces the XPL 'second skin'.

The placebo control (the vehicle-treated group) comprised a similar two-step formulation from which the catalyst was removed to prevent network cross-linking. The blinded and trained graders found significant improvements in bag severity at 1 and 4 hours after XPL application (Figure 6d). The modest and statistically non-significant improvement from baseline in the vehicle-treated sites are likely due to the skin hydration properties of XPL and/or to the light scattering ingredients incorporated in the vehicle delivery of our two-step system. At one hour following test article application, both the XPL and the vehicle groups showed improvements in their average wrinkle severity grade, which did not differentiate the effect of the XPL and the vehicle (not significant). At four hours, the continued improvement at the XPL-treated sites was observed to exceed the effects perceived at the vehicle-treated sites ($p<0.0001$). Examples correlating the improvement of the lower lid following XPL application to the underlying changes in skin hydration are shown by pairing photographs with the corresponding OCT images (Figure 6).

Over the course of four hours, the XPL-treated sites were significantly smoother than the vehicle control sites (Figure 6e, 2.18×10^{-2} versus 3.89×10^{-2}, respectively, $p<0.01$). The surface irregularity (SI) calculations also suggested a transient improvement in surface smoothness for the vehicle-treated sites compared to the baseline at 1 hour ($p<0.001$), which was likely an effect of hydration. By 4 hours, however, the vehicle-treated site SI approached the corresponding baseline value, while the XPL-treated sites sustained their surface smoothness relative to baseline ($p<0.0001$). This result is consistent with the visual assessment of a smoother skin surface with fewer irregularities at 4 hours after XPL application, compared to the vehicle.

The OCT images were further analyzed to quantify the change in pixel intensity resulting from the XPL and the vehicle treatments. Lucent pixels depict regions of low water content, whereas dark pixels indicate regions of increased hydration (Figure 6). Within the viable epidermis, there was a significant decrease ($p<0.00001$, see Table 2) in the OCT pixel intensity during the 4 hours following the XPL application compared the baseline values (Figure 6a-c) which we hypothesize

was due to the enhanced skin barrier imposed by XPL wear, as suggested by the TEWL measurements. At 4 hours, the average intensity for the XPL sections analyzed was 10% lower than for the vehicle sections ($p<0.0001$, see Table 2), further supporting our interpretation that the XPL wear increases skin hydration.

In another study evaluating the XPL durability, 23 out of 25 subjects demonstrated excellent film integrity at the end of a 16-hour wear period. Two of the 25 subjects showed a visible film boundary at the lower lid application site, although the XPL remained intact and adherent to the skin. Repeated daily wear resulted in no report of irritation or other adverse events resulting from the XPL use. Furthermore, the XPL remained intact following activities such as swimming, running, and exposure to rain.

DISCUSSION

We report here that a novel, two-step, flowable polysiloxane-based formulation, applied topically and cross-linked *in-situ* to form an "invisible" thin film on human skin, can provide a durable, skin-conforming elastic 'second skin'. This 'second skin' is wearable, moisturizing, safe, well-tolerated, and provides enhanced mechanical integrity to the underlying skin.

The XPL material design criteria for tensile modulus and elastic recoil were selected to mimic youthful skin properties, while the extent of elongation was selected to provide comfort through the range of motion the skin experiences. The material described here demonstrated a tensile modulus of 0.5 MPa, which was designed to cover the range of elastic response in normal healthy skin reported in the literature[24,25]. Such elastic recoil behaviour, together with a 250% elastic strain region until fracture demonstrated by this material, are likely design parameters that promote the seamless integration of the XPL at the skin interface, thereby allowing for even extreme ranges of motion while providing the instantaneous recoil that is characteristic of youthful, intact skin.

The proof-of-concept human studies showed that XPL contraction reliably reshapes the skin surface, as well as mechanically flatten herniated fat pads that cause under-eye bagging. A double-blind, randomized, placebo controlled study documented a marked decrease in under-eye bag severity and wrinkling that was significantly greater than that produced by the same

composition without the catalyst for cross-linking (vehicle-treated control), and hence, not attributable to the product moisturizing properties alone. A significant increase in the surface smoothness was also measured for the skin sites exposed to the XPL compared to the vehicle. Together, the double-blinded studies distinguish the contractile, mechanical effects achieved by the XPL cross-linked polysiloxane network on the cosmetic appearance of the skin from the vehicle effects that likely arise from skin hydration and optical manipulation of the skin surface. The visible flattening of the lower lid fat pad following 3 hours of XPL application would also suggest that internal stress, or the XPL shrinkage, resulting from the volatiles loss is another important design parameter deserving additional characterization for effecting changes in skin shape.

The XPL also significantly decreased moisture loss from the skin, as evidenced by OCT imaging that quantified the increased state of epidermal hydration at sites exposed to the XPL. The OCT measurements were further supported by the quantitative measures of transepidermal water loss (TEWL). Of note, the XPL performed better than a leading commercial moisturizer and a conventional highly occlusive agent, petrolatum, over the course of 24 hours. Indeed, the elasticity and durability of XPL film on skin should also contribute to consistent barrier properties of the film, during wear. By comparison, the topical creams such as petrolatum or inelastic film formers such as polyurethane UR450 display plastic deformation which potentially may impact a decrease in the coating uniformity during wear. These localized variations in the film integrity may produce 'weak spots' that comprise barrier protection.

Overall, the observed elastic skin 'memory' is hypothesized to result from the XPL-induced increases in skin hydration and/ or the transient changes to the underlying skin tensile properties while interfacing the tangential XPL contractile stresses imposed at the skin surface. The potential of the XPL to impose a mechanical skin 'memory' that translates to a transient change in the underlying skin mechanical behaviour, following removal of the XPL will be the subject of future studies examining the long term benefits to skin following daily, repeated XPL wear. The association between anisotropic skin mechanical behavior and the Langer lines is well documented in the literature[26]. Skin anisotropy and the loss of skin mechanical integrity with age have been attributed to changes in the elastin and collagen architecture that constitute the

dermis. The application of a thin, contractile layer to the stratum corneum leads to isotropic, tangential stresses exerted by the XPL in the plane of the skin. The role of these tangential stresses on modulating the anisotropic skin stress tensor deserves additional investigation. New devices that measure the in-plane stresses inherent to skin have further reinforced the anisotropic tension underlying skin mechanics[31] and may be leveraged to characterize the in-plane mechanical changes induced by the XPL. Moreover, coupling these new techniques with additional detailed analyses of skin adhesion and the histology associated with the skin biomechanical responses utilizing human skin explant models may provide additional insight to the XPL-induced changes on the skin architecture. The elucidation of the mechanisms underlying the observed changes in the bulk skin mechanical behaviour resulting from the introduction of a thin skin-conforming layer at the surface, along with ongoing efforts to delineate the associated spatial changes in skin geometry, may offer additional insights in the material design criteria required for target indications addressed by the next generation XPLs.

A wearable material layer that restores the normal skin mechanics and appearance is unprecedented and provides a platform to solve other cutaneous problems. While the focus of this work has been to elucidate the impact of the elasto-mechanical properties of the XPL on skin, further directions of research and improvement could be envisioned to create better products for barrier protection and cosmetics. One such improvement might include extending the XPL wear beyond the current once-daily application specification. In addition, skin-adherent and skin-conforming polymers utilizing a similar concept could be developed as durable UV-protection or as concealers of vascular anomalies such as port-wine stains. Devices that deliver pharmaceutical actives or assay biomarkers at the skin surface are additional potential applications. In summary, the XPL ‘second skin’ concept described here could potentially yield a next generation of functionalized second skins with broad medical benefits while allowing skin to look and behave naturally.

ACKNOWLEDGEMENTS

The authors thank Gary Grove, PhD and Zoe Diana Draelos, MD for their helpful discussions and M. Su for her assistance with the *in-vivo* use studies.

AUTHOR CONTRIBUTION

BY, SYK, FHS, BAG, and RRA contributed to the design and analysis of the *in-vivo* use studies. AA, NR, and MP conducted the materials synthesis and characterization studies. AA, NR, MP, AN, and DGA contributed to the analysis of the *in-vitro* mechanical characterization data. SYK supervised the execution of the *in-vivo* use studies. AP conducted *in-vivo* Study B. BY and RL managed the research efforts. BY, AA, AN, BAG, RRA, and RL wrote the manuscript with the help of the co-authors.

COMPETING FINANCIAL INTEREST

Personal financial interests:

BY, AA, NR, MP, AP were employees at Living Proof, Inc. and own Living Proof stocks.

SYK is currently an employee at Living Proof and owns Living Proof stocks.

AA, NR are currently employees at Olivo Laboratories, LLC. and own shares from Olivo Laboratories, LLC.

AN, DGA, BAG, RRA, RL own stocks from Living Proof, Inc.

AN, DGA, FHS, RRA, RL own shares from Olivo Laboratories, LLC.

FHS, BAG received consultation fees from Living Proof, Inc.

FHS received consultation fees from Olivo Laboratories, LLC.

The following patents and patent applications belong to Living Proof, Inc.

US8,691,202; WO2012/030984; US2014/0044670; US2013/0078209; WO2013/044098.

FIGURES and TABLES

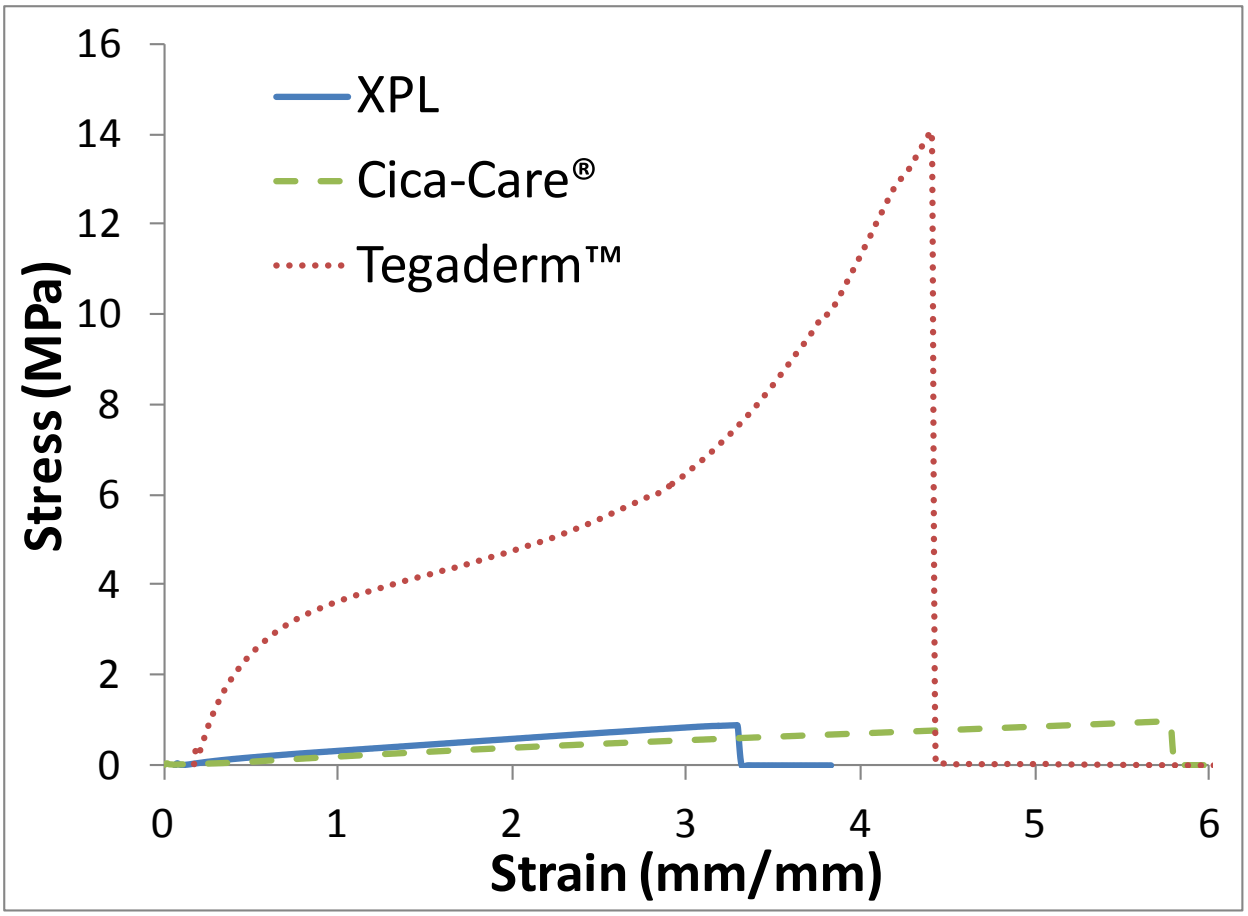

Figure 1a: Tensile stress-strain plots for XPL and two commercial pre-formed wound dressings: Cica-Care® silicone sheet and Tegaderm™ polyurethane sheet with acrylic adhesive backing. Topically applied XPL and pre-formed Cica-Care® silicone sheet display good elastic recoil until break. In contrast, pre-formed Tegaderm™ polyurethane sheets display plastic deformation profiles that yield after 15% strain.

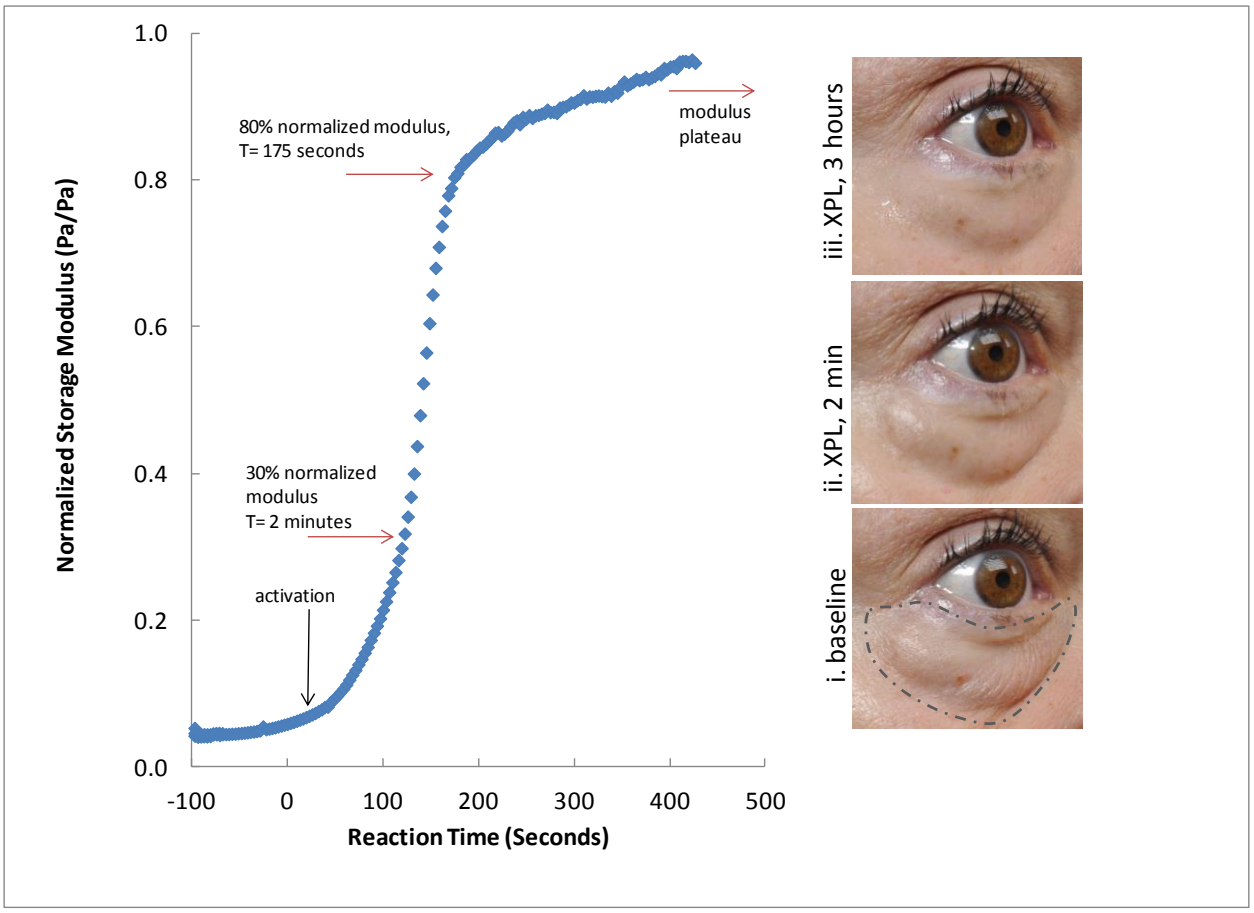

Figure 1b: XPL cross-linking kinetics. Cross-linking kinetics of topical Step 1 formulation containing active prepolymers was represented by the normalized XPL storage modulus as a function of reaction time. The S-shape curve was obtained using the rheometer test for cross-linking kinetics (see Materials and Methods). Moduli are normalized by the storage modulus measured at the last time point. In the method, three distinct regions of the reaction are observed with respect to the rate of increase in storage modulus (the slope of the reaction curve). The first region captures the catalyst-stabilizer effect, where the reaction is suppressed by chemically stabilizing the platinum catalyst to allow sufficient sample preparation time before the rheometer records the beginning of the actual cure kinetics. The steep increase in the storage modulus after 200 seconds signals the rapid cross-linking from hydrosilylation over the next 100 seconds. After 300 seconds, the storage modulus increases asymptotically as the cross-linking reaction approaches completion. Photographs illustrating the impact of modulus build on compressing the herniated fat pad are shown. (i) Prominent fat pad protrusion (lower lid bag severity grade 4 is defined by the concavity at the lower tear trough at baseline). XPL was applied to the region demarcated by the dashed line. (ii) Two minutes following XPL application, the skin texture appeared smoother and the skin laxity seen by the mild skin wrinkling at the medial and central fat pads appeared tightened. (iii) At 3 hours following XPL application, the peak compression shows a 2-grade improvement in bag severity using a standardized scoring system.

Figure 2: The visual impact of a 2-grade improvement (from grade 3 to grade 1) after applying XPL to the under-eye area. This image is an illustrative example of a 2-grade improvement, which was consistently observed following repeated split face application of XPL (n > 10).

Figure 3: Time-lapse photos extracted from video footage of skin retraction following a dermatological tenting test. XPL was applied to the right side. The left side served as the untreated control. The four frames extracted show the left and the right side (a) before tenting, (b) during the tenting test (gentle pinch), (c) immediately after skin is released, and (d) 3 seconds after the skin is released. The side wearing the XPL demonstrates zero plastic strain and retracts to the original position, whereas the untreated side demonstrates poor elastic recoil and sustained the plastic strain resulting from the imposed stress. These results were consistent with repeated tenting studies (n>10).

Figure 4: Pilot study evaluating XPL induced changes in skin elasticity (Study 1) when worn over 24 hours on normal volar forearm skin. (a) At baseline, a representative plot of the negative pressure required to extend the skin to a fixed height using the suction cup method is shown. The two distinct regions highlighted in red and blue, correspond to the viscoelastic and the elastic skin response regions, respectively. The hysteresis experienced following each skin distension cycle is shown by the dotted blue line. (b) Following 24 hours of XPL wear, the treated skin sites demonstrated increased elastic behavior, showing a linear elongation response with time (blue squares) for the same representative skin sites. Thirty minutes following XPL removal, after 24 hours of wear (solid diamonds), the skin approached the baseline behavior. (c) The average skin retraction time was measured for 6 different individuals. The three treatments were applied to each arm, yielding duplicate treatment sites assigned using a predetermined rotational scheme for each subject. The sites exposed to XPL demonstrated a marked decrease in the skin retraction time (from 838 ± 164 ms to 533 ± 57 ms, $p<0.005$, paired Student's t-test) compared to the baseline values, unlike the 12% lactic acid moisturizer applied twice, initially and after 12 hours (879 ± 174 ms to 851 ± 164 ms, NS) and the untreated control sites (893 ± 140 ms to 795 ± 104 ms, NS). Thirty-five minutes after XPL removal, the skin recoil time and the corresponding elongation pressures returned to the baseline values. The negative pressure recorded at 12% distension similarly decreased 29% (from 382 ± 42 kPa to 273 ± 22 kPa). The error bars represent the standard errors of mean (SEM). Data sets marked with asterisks (*) represent statistically significant differences using a paired Student's t-test.(d) in the same 6 subjects, $p<0.05$) compared to the baseline values, unlike the twice treated moisturizer sites (418 ± 27 kPa to 396 ± 23 s, NS) and the untreated control sites (432 ± 39 kPa to 423 ± 39 kPa, NS). (e) Changes in skin hydration were evaluated in 24 subjects following application of XPL and petrolatum with post-hoc analysis (Tukey method, $\alpha=0.05$). XPL (116.65 µS at 1 hr) demonstrated significant increases in skin hydration compared to petrolatum (P) (42.65 µS at 1 hr) ($p<0.05$), and untreated control sites (UC) (21.95 µS at 1 hr) ($p<0.001$).

(a)

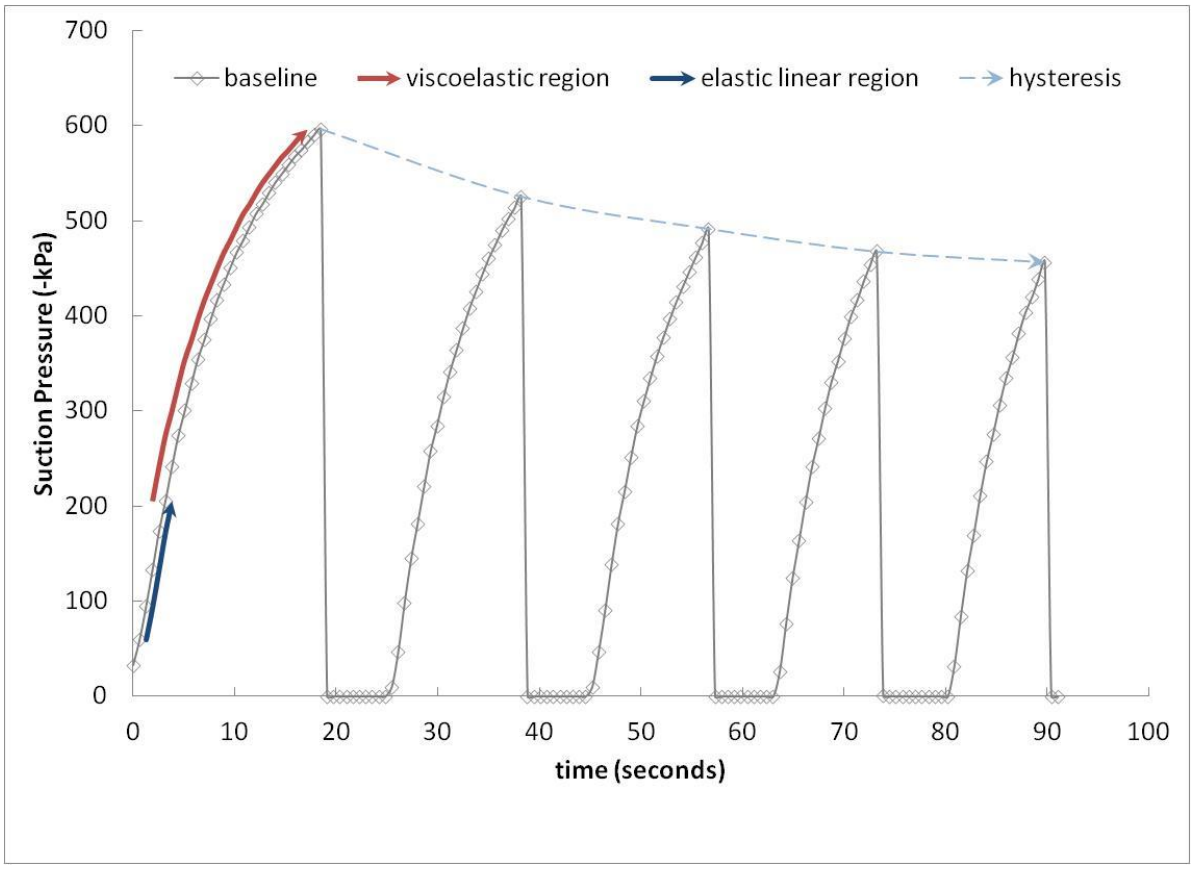
baseline
viscoelastic region
elastic linear region
hysteresis
Suction Pressure (-kPa)
700
600
500
400
300
200
100
0
0
10
20
30
40
50
60
70
80
90
100
time (seconds)

(b)

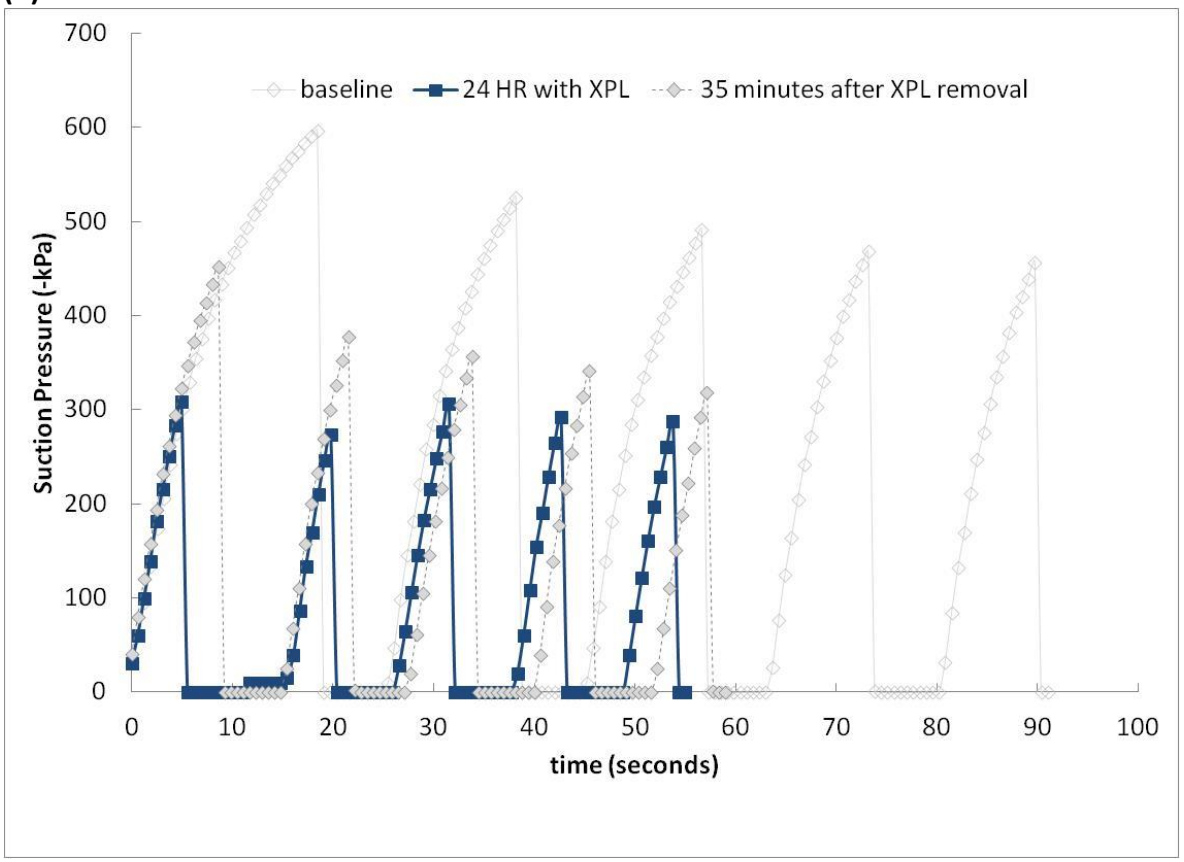
baseline
24 HR with XPL
35 minutes after XPL removal
Suction Pressure (-kPa)
700
600
500
400
300
200
100
0
0
10
20
30
40
50
60
70
80
90
100
time (seconds)

(c)

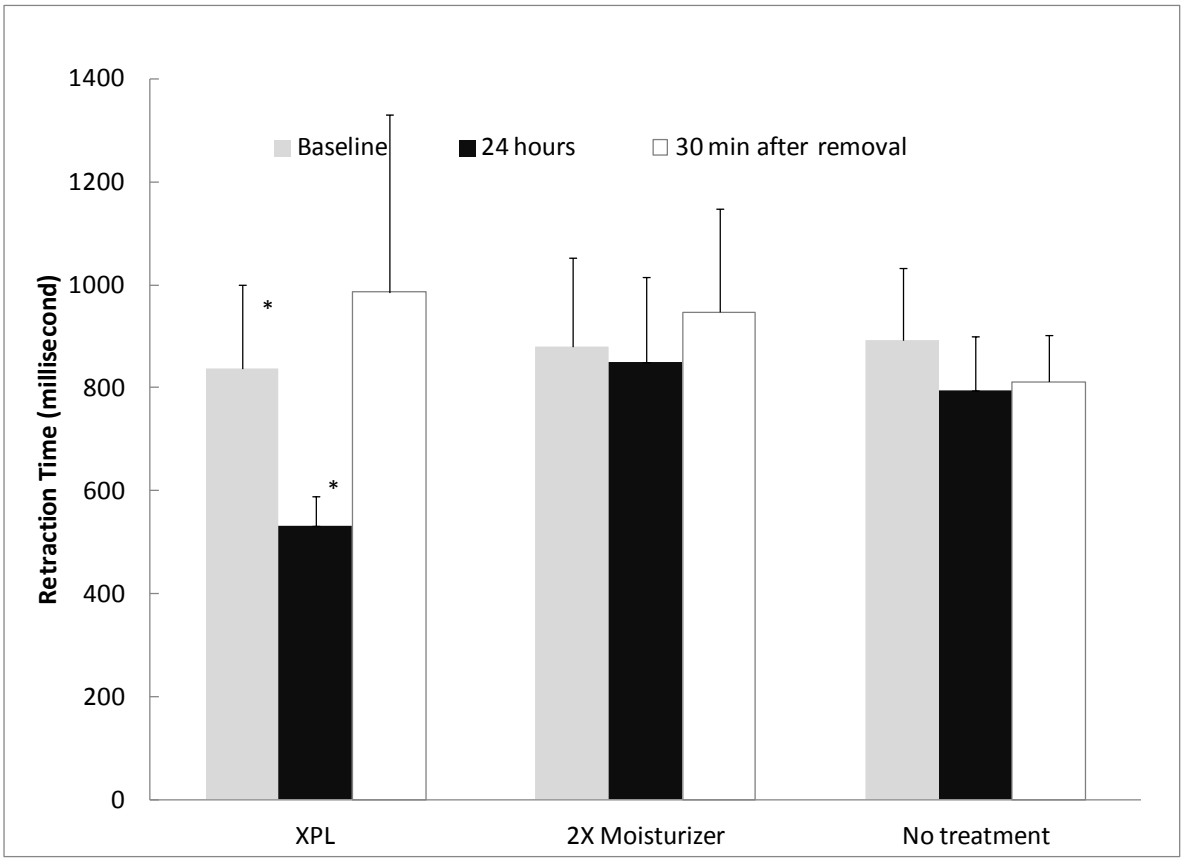
1400
1200
1000
800
600
400
200
0
Retraction Time (millisecond)
Baseline
24 hours
30 min after removal
*
*
XPL
2X Moisturizer
No treatment

(d)

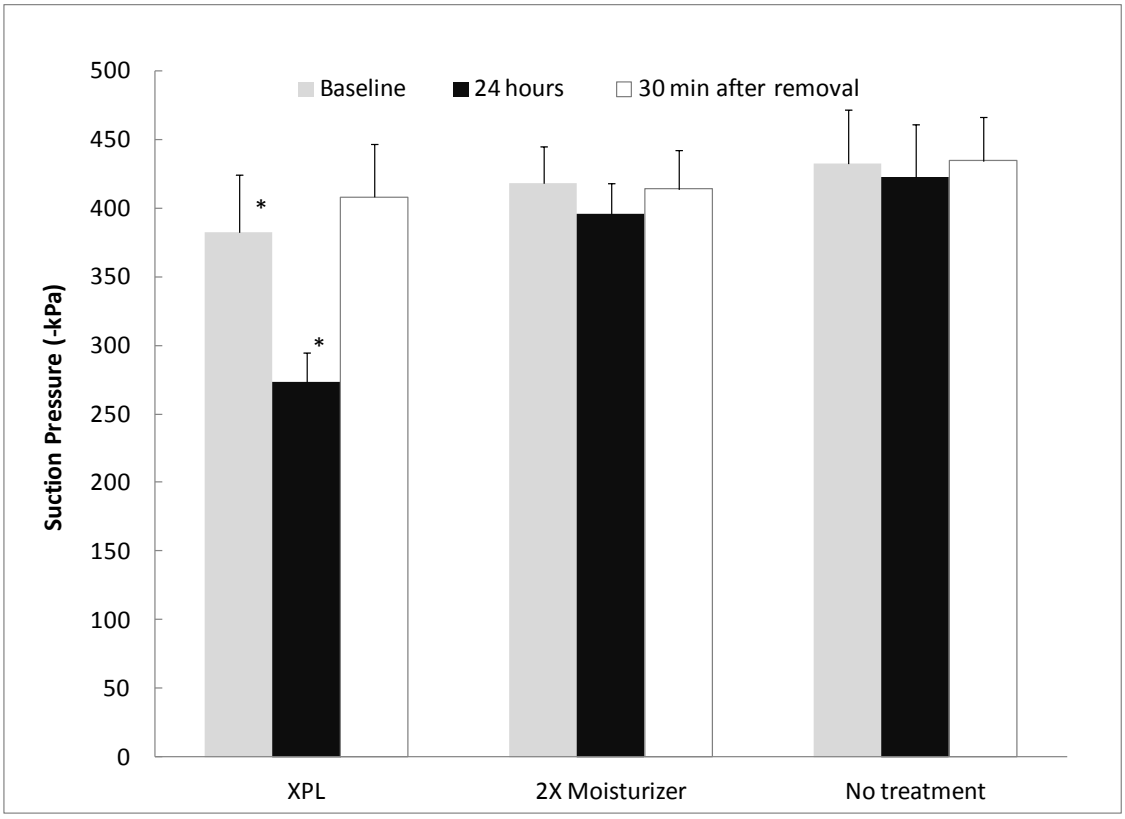
Baseline
24 hours
30 min after removal
Suction Pressure (-kPa)
500
450
400
350
300
250
200
150
100
50
0
*
*
XPL
2X Moisturizer
No treatment

(e)

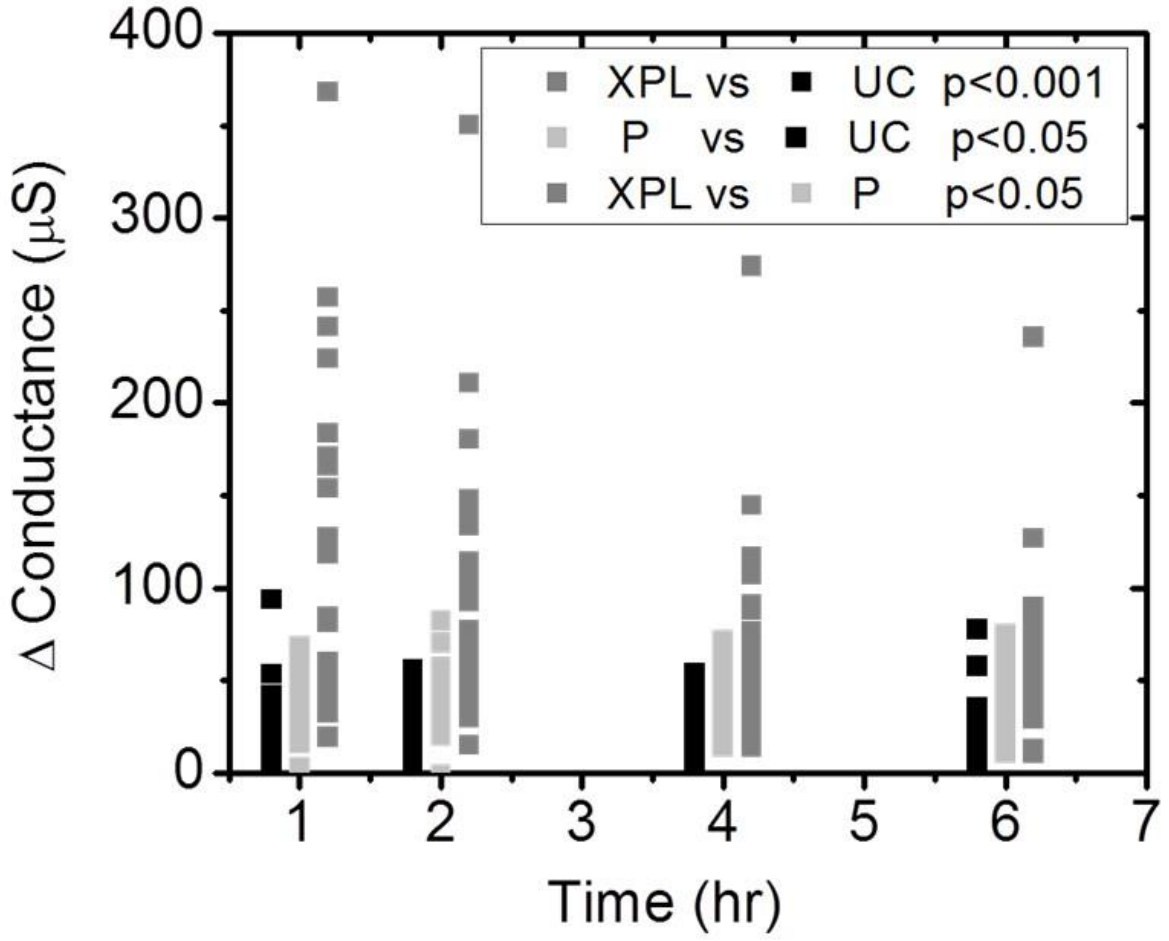
400
300
200
100
0
Δ Conductance (μS)
1
2
3
4
5
6
7
Time (hr)
XPL vs UC p<0.001
P vs UC p<0.05
XPL vs P p<0.05

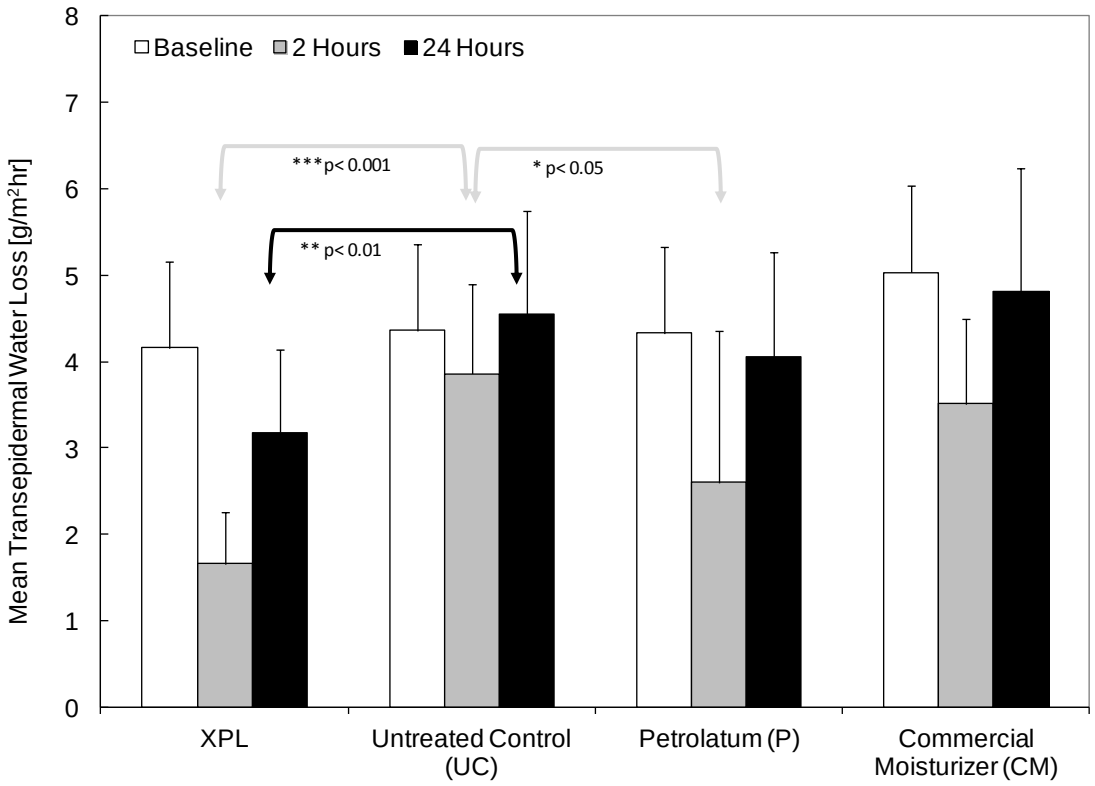

Figure 5: Study C. Clinical data showing enhanced skin barrier function and sustained skin hydration for subjects (N=22) with dry skin. At two hours, the sites treated with petrolatum (P) and XPL demonstrated significantly reduced transepidermal water loss (TEWL) values compared to the untreated control (UC) values ($^{*}p<0.05$ and $^{**}p<0.001$). A reduction in the transepidermal water loss was sustained with the XPL over the course of 24 hours ($^{***}p<0.01$). At 24 hours, the differences measured for P and for CM were not statistically significant when compared to the UC. The error bars represent one standard deviation from the mean. The p-vales were calculated based on one-way ANOVA analyses.

Figure 6a, 6b, 6c: Representative three-dimensional photography and non-invasive imaging of the underlying epidermal layers using optical coherence tomography are shown for three subjects at baseline and 4 hours after XPL application. The blue and red lines illustrate the two lengths used to calculate the SI. The 3 vertical pairs of metallic markers that were placed along the lower lid delineate the 3 different OCT measurement sites that were evaluated at each side. The two arrows in the OCT image correspond to the placement of one pair of markers. After 4 hours, it is possible to visualize the XPL film over the stratum corneum. The stratum corneum (SC), epidermis (E), dermis (D) and XPL regions are identified in panel (a). Pixel intensity analysis of the 3 OCT sections acquired at each application side at each time point for the 12 subjects suggested an greater level of hydration resulting from the XPL application compared to the vehicle at 4 hours (25888 ± 3207 versus 28774 ± 3535, respectively, $p<0.0001$, paired Student's t-test), where lower pixel intensities represent a greater fraction of dark pixels, indicative of high water content. At baseline, the average pixel intensities measured were 31477 ± 3708 (XPL) and 30878 ± 3821 (vehicle), translating to decreases of 18% and 7% in the pixel intensities respectively.

(a)

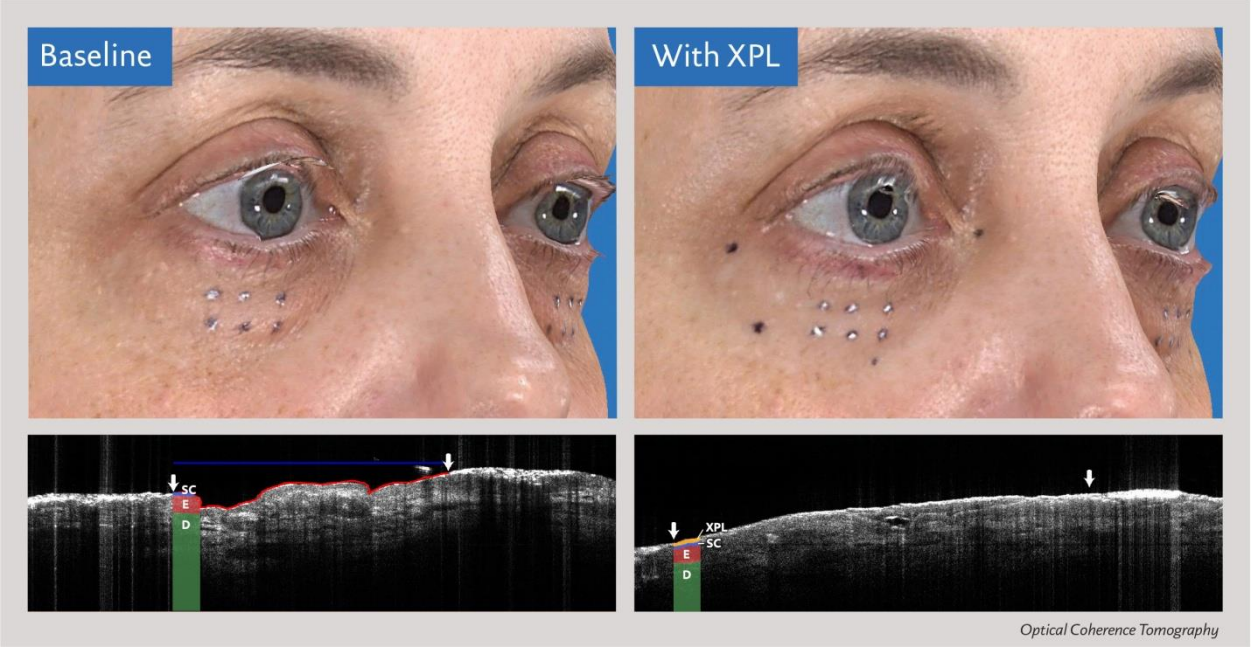

(b)

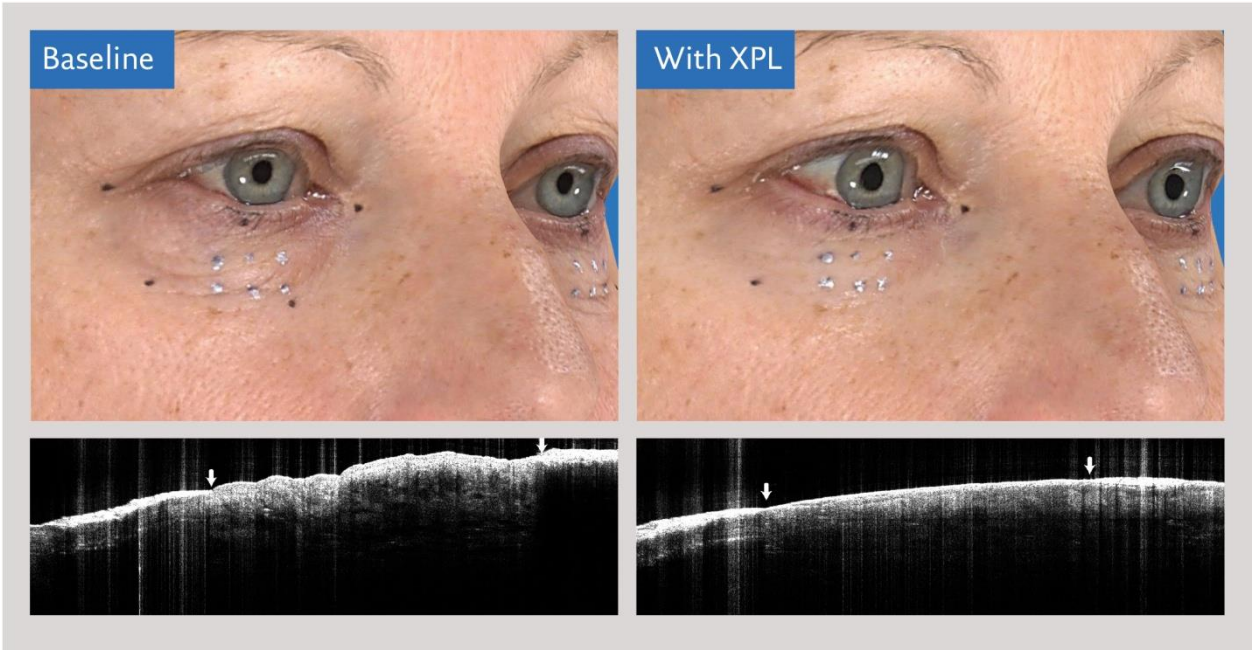

(c)

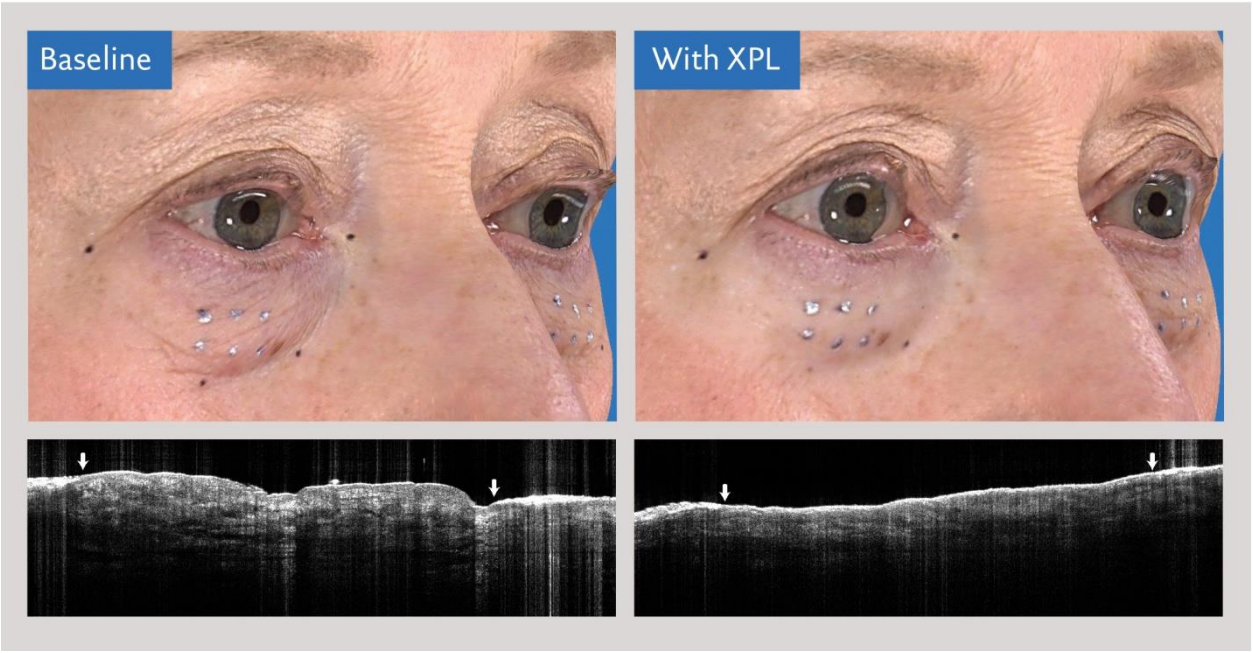

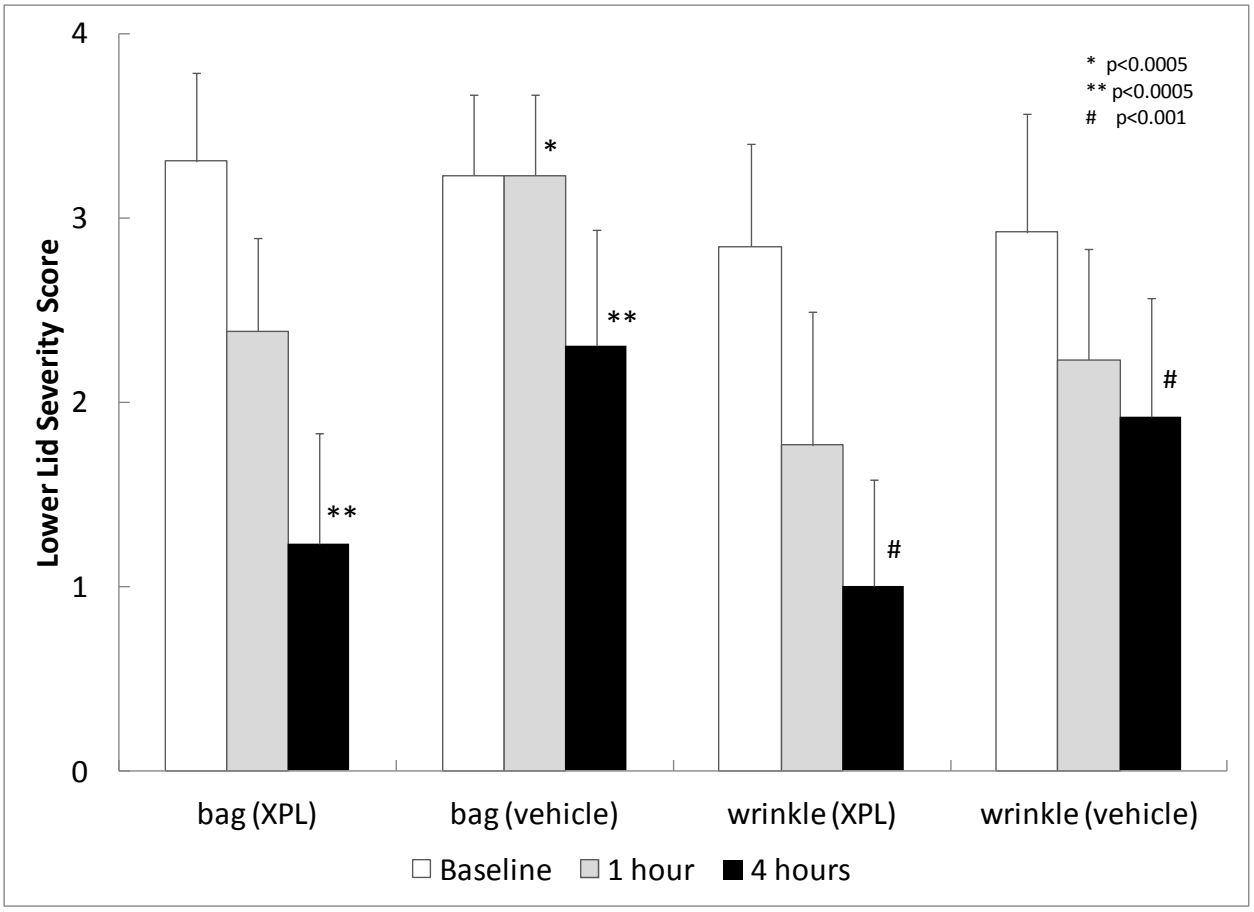

Figure 6d: Double blind, randomized, placebo controlled pilot clinical to evaluate XPL contractile function at the lower lid using 0-4 photonumeric scales for quantifying extent of skin response. At 1 hour (2.38 ± 0.51) and at 4 hours (1.23 ± 0.60) following test article application, the XPL demonstrated statistically significant ($p<0.0005$) one grade and two grade improvements compared to the corresponding vehicle grades of 3.23 ± 0.44 and 2.31 ± 0.63, respectively. The baseline average values for the XPL and the vehicle sites were 3.31 ± 0.48 and 3.23 ± 0.44, respectively. The lower lid wrinkle values for the vehicle at baseline, 1 hour and 4 hours are 2.92 ± 0.64, 2.23 ± 0.60, and 1.92 ± 0.64, respectively. For the XPL treatment sites, the wrinkle grades at the corresponding time points are 2.85 ± 0.55, 1.77 ± 0.73 and 1.0 ± 0.58, respectively. At four hours, a significant improvement in wrinkles was observed ($p<0.001$) for the XPL side compared to the vehicle. The error bars represent one standard deviation (SD) of the mean. The symbols (*, **, #) identify data sets demonstrating statistical differences using a paired Student's t-test.

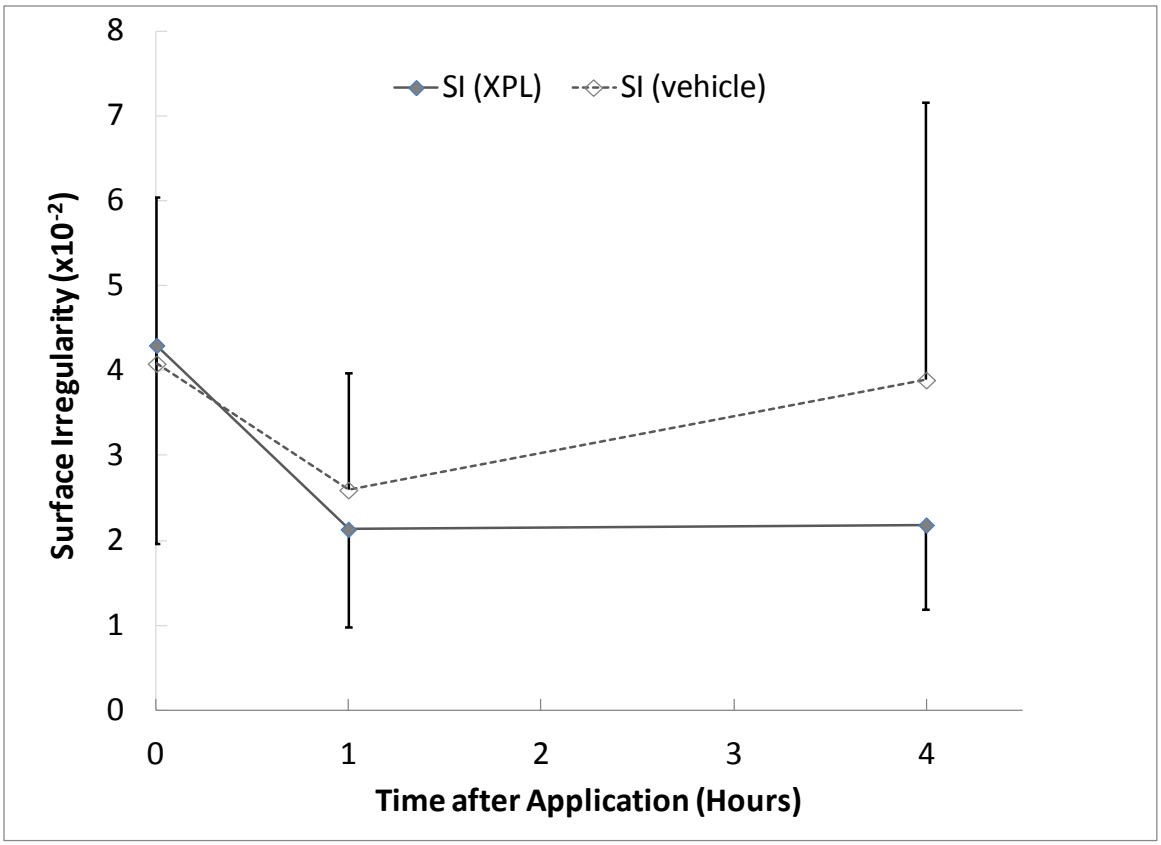

Figure 6e: The Surface Irregularity (SI) values measured from the triplicate OCT images obtained at each treatment side show significantly decreased skin surface roughness at four hours following XPL application compared to the vehicle control ($2.18x10^{-2} \pm 1.00x10^{-2}$ versus $3.89x10^{-2} \pm 3.27x10^{-2}$, respectively, $p<0.01$). Zero SI values correspond to smooth surfaces with no measurable roughness. Baseline SI values showed no significant differences between the two groups ($4.30x10^{-2} \pm 2.34x10^{-2}$ versus $4.08x10^{-2} \pm 1.96x10^{-2}$, respectively), validating the randomization scheme utilized. At one hour, the difference measured between the two groups trended toward significance ($2.13x10^{-2} \pm 1.16x10^{-2}$ versus $2.59x10^{-2} \pm 1.38x10^{-2}$, respectively, $p=0.18$). The error bars denote one standard deviation of the mean. The p-values were calculated using paired Student's t-tests.

REFERENCE

1. Irvine, A. D., McLean, W. H. & Leung, D. Y. Filaggrin mutations associated with skin and allergic diseases. *N. Engl. J. Med.* **365**, 1315-1327 (2011).
2. Schon, M. P., Boehncke, W. H. & Brocker, E. B. Psoriasis: Clinical manifestations, pathogenesis and therapeutic perspectives. *Discov. Med* **5**, 253-258 (2005).
3. Schon, M. P. & Boehncke, W. H. Psoriasis. *N. Engl. J. Med.* **352**, 1899-1912 (2005).
4. Bieber, T. Atopic dermatitis. *N. Engl. J. Med.* **358**, 1483-1494 (2008).
5. Yosipovitch, G. & Bernhard, J. D. Clinical practice. Chronic pruritus. *N. Engl. J. Med.* **368**, 1625-1634 (2013).
6. Gilchrest, B. A. Skin aging and photoaging: an overview. *J. Am. Acad. Dermatol.* **21**, 610-613 (1989).
7. Balin, A. K. & Pratt, L. A. Physiological consequences of human skin aging. *Cutis* **43**, 431-436 (1989).
8. Anderson, R. R. Lasers for dermatology and skin biology. *J. Invest. Dermatol.* **133** (2013).
9. Rushmer, R. F., Buettner, K. J., Short, J. M. & Odland, G. F. The skin. *Science* **154**, 343-348 (1966).
10. Kim, D. H., Xiao, J., Song, J., Huang, Y. & Rogers, J. A. Stretchable, curvilinear electronics based on inorganic materials. *Adv. Mater.* **22**, 2108-2124 (2010).
11. Rogers, J. A., Someya, T. & Huang, Y. Materials and mechanics for stretchable electronics. *Science* **327**, 1603-1607, doi:10.1126/science.1182383 (2010).
12. Jang, K.-I., Chung, H. U., Xu S., Lee, C. H., Luan, H., Jeong, J., Cheng, H., Kim, G.-T., Han, S. Y., Lee, J. W., Kim, J., Cho, M., Miao, F., Yang, Y., Jung, H. N., Flavin, M., Liu, H., Kong, G. W., Yu, K. J., Rhee, S., Chung, J., Kim, B., Kwak, J. W., Yun, M. H., Kim, J. Y., Song, Y. M., Paik, U., Zhang, Y, Huang, Y. & Rogers, J. A. Soft Network composite materials with deterministic and bio-inspired designs. *Nature Comm.* **6**:6566 (2015).
13. Mitragotri, S., Blankschtein, D. & Langer, R. Ultrasound-mediated transdermal protein delivery. *Science* **269**, 850-853 (1995).
14. Kost, J., Mitragotri, S., Gabbay, R. A., Pishko, M. & Langer, R. Transdermal monitoring of glucose and other analytes using ultrasound. *Nature Med.* **6**, 347-350 (2000).
15. Xu, S., Zhang, Y., Jia, L., Mathewson, K. E., Jang, K.-I., Kim, J., Fu, H., Huang, X., Chava, P., Wang, R., Bhole, S., Wang, L., Na, Y. J., Guan, Y., Flavin, M., Han, Z., Huang, Y. & Rogers, J. A. Soft microfluidic assemblies of sensors, circuits, and radios for the skin. *Science* **344**, 70-74 (2014).
16. Clark, R. A., Ghosh, K. & Tonnesen, M. G. Tissue engineering for cutaneous wounds. *J. Invest. Dermatol.* **127**, 1018-1029 (2007).
17. Meddahi-Pellé , A., Legrand, A., Marcellan, A., Louedec, L., Letourneur, D. & Leibler, L. Organ Repair, Hemostasis, and In-vivo Bonding of Medical Devices by Aqueous Solutions of Nanoparticles. *Angew. Chem. Int. Ed. Engl.* **53**, 6369-6373 (2014).
18. Davis, S. C., Gil, J., Treu, R., Valdes, J., Solis, M., Eberlein, T. & Eaglstein, W. H. The healing effect of over-the-counter (OTC) wound healing agents applied under semi-occlusive film dressing. *Br. J. Dermatol.*, **172**(2):544-6 (2015).
19. Borde, A., Larsson, M., Odelberg, Y., Hagman, J., Lowenheilm, P. & Larsson, A. Increased water transport in PDMS silicone films by addition of excipients. *Acta Biomater.* **8**, 579-588 (2012).

20. Hammock, M. L., Chortos, A., Tee, B. C., Tok, J. B. & Bao, Z. 25th anniversary article: The evolution of electronic skin (e-skin): a brief history, design considerations, and recent progress. *Adv. Mater.* **25**, 5997-6038 (2013).
21. Webb, R. C., Bonifas, A. P., Behnaz, A., Zhang, Y., Yu, K. J., Cheng, H., Shi, M., Bian, Z., Liu, Z., Kim, Y.-S., Yeo, W.-H., Park, J. S., Song, J., Li, Y., Huang, Y., Gorbach, A. M. & Rogers, J. A. Ultrathin conformal devices for precise and continuous thermal characterization of human skin. *Nature Mater.* **12**, 938-944 (2013).
22. Linear Polydimethylsiloxanes CAS No. 63148-62-9 (European Centre for Ecotoxicology and Toxicology of Chemicals, Brussels, Belgium, 2011).
23. Lewis, L. N., Stein, J., Gao, Y., Colborn, R. E. & Hutchins, G. Platinum Catalysts Used in the Silicones Industry. Their synthesis and activity in hydrosilylation. *Platin. Met. Rev.* **41**, 66-75 (1997).
24. Annaidh, A. N., Bruyere, K., Destrade, M., Gilchrist, M. D. & Ottenio, M. Characterization of the anisotropic mechanical properties of excised human skin. *J. Mech. Behav. Biomed. Mater.* **5**, 139-148 (2012).
25. Agache, P. G., Monneur, C., Leveque, J. L. & Rigal, J. D. Mechanical Properties and Young's Modulus of Human Skin in Vivo. *Arch. Dermatol. Res.* **269**:221-232 (1980).
26. Hendriks, F. M., Brokken, D., van Eemeren, J. T., Oomens, C. W., Baaijens, F. P. & Horsten, J. B. A numerical-experimental method to characterize the non-linear mechanical behaviour of human skin. *Skin Res. Technol.* **9**, 274-283 (2003).
27. Manschot, J. F. & Brakkee, A. J. The measurement and modelling of the mechanical properties of human skin in-vivo--II. The model. *J. Biomech.* **19**, 517-521 (1986).
28. Diridollou, S., Patat, F., Gens, F., Vaillant, L., Black, D., Lagarde, J. M., Gall, Y. & Berson, M. In vivo model of the mechanical properties of the human skin under suction. *Skin Res. Technol.* **6**, 214-221 (2000).
29. Cua, A. B., Wilhelm, K. P. & Maibach, H. I. Elastic properties of human skin: relation to age, sex, and anatomical region. *Arch. Dermatol. Res.* **282**, 283-288 (1990).
30. Kraft, J. N. & Lynde, C. W. Moisturizers: what they are and a practical approach to product selection. *Skin Therapy Lett.* **10**, 1-8 (2005).
31. Boyer, G., Molimard, J., Tkaya, M. B., Zahouani, H., Pericoi, M. & Avril, S. Assessment of the in-plane biomechanical properties of human skin using a finite element model updating approach combined with an optical full-field measurement on a new tensile device. *J. Mech. Behav. Biomed. Mater.* **27**, 273-282 (2013).
32. Pedersen, L. & Jemec, G. B. Mechanical properties and barrier function of healthy human skin. *Acta Derm. Venereol.* **86**, 308-311 (2006).
33. Gniadecka, M. & Serup, J. in *Handbook of Noninvasive Methods and the Skin* (ed J. Serup, Jemec, GBE) pages 329-335 (CRC Press, Boca Raton, FL, 2006).

METHODS

XPL Two-Step Delivery System Formulation Development

To coat the skin with a thin and uniform layer of the lead RPB, formulation design efforts focused on the development of a novel emulsion system comprising an aqueous-compatible internal phase and a siloxane-compatible external phase. The formulation development efforts required the incorporation of an internal phase thickener that enabled the appropriate shear-thinning effects to facilitate the deposition of the siloxane phase. If the siloxane phase was deposited too rapidly onto the skin, the uniformity of the XPL was compromised, while a prolonged application 'playtime' interfered with the mechanical integrity of the cross-linked layer. Moreover, we constrained the total amount of non-volatile silicone-compatible ingredients that could act as plasticizers in the final XPL film to 2% (w/w) or less. Optimization of the formulation flow properties and the siloxane deposition time was achieved by adjusting the emulsifier and thickener chemistries, as well as the overall ingredient compositions, to provide a novel delivery system that maintained the above RPB mechanical-adhesive attributes for the *in-situ* cross-linked XPL film.

After multiple rounds of formulation optimization, a two-step delivery system comprising the "Step 1" and "Step 2" formulations was developed. Water-in-silicone emulsion systems were developed to enable the delivery of the lead RPB (at 32% w/w) of Step1 and the platinum catalyst (at 200 ppm w/w) of Step 2 through the continuous silicone phase. With this approach, Step 1 facilitated a consistent deposition of the lead RPB coating on skin that was subsequently cross-linked *in-situ* to form the XPL film when exposed to the platinum catalyst in Step 2. The authors are not aware of other topical emulsion-based formulations that successfully incorporate such a high concentration of silica-reinforced polysiloxanes.

The Step 1 formulation containing the lead RPB demonstrated improved spreading properties on lax skin compared to the lead RPB alone. Plots of the instantaneous viscosity as a function of the shear rate illustrated a stronger shear-thinning effect of the Step 1 formulation containing the lead RPB, compared to the lead RPB alone, with a 2- to 3-fold decrease in the instantaneous viscosity at shear rates above 5 sec^{-1} (Figure 8 in Supplementary Information). Note that maximum shear rates from 10^4 to 10^5 sec^{-1} have been reported for the application of topical

cream products on skin[28]. The rheological behaviour of Step 1 allows the emulsion to exhibit lower viscosities at the high shear rates associated with topical formulation application, despite the comparable viscosities of 1,500 Pa.s (Step 1 containing the lead RPB) and 1,800 Pa.s (the lead RPB alone) measured at low shear rate of 0.15 sec^{-1}. In addition, the high formulation viscosities measured at low shear rates support prolonged shelf-life stability by lowering the rates of gravity-driven sedimentation.

Finally, the XPL optical properties were adjusted to complement the light scattering properties of natural skin. The XPL optics were modulated by introducing light scattering particles into the Step 2 formulation such that these particles were deposited at the XPL surface. Surface-treated nylon particles with a particle diameter approximating 8 microns and a refractive index of 1.54 (Nylon 10-I2, KOBO Products, Inc., South Plainfield, NJ) provided the best optical match between the XPL and natural skin, following repeated clinical evaluation of several commercially available light scattering particles. Clinical examples of the optical effects are shown in Figure 1b, Figure 2, Figure 3, and Figure 6.

Materials

Vinyl dimethicone, hydrogen dimethicone, and Karstedt platinum catalyst were purchased from AB Specialty Silicones (Waukegan, IL). PMX-1184 (polydimethylsiloxane and disiloxysilane), FZ-2233 (Bis-Isobutyl PEG/PPG-10/7/Dimethicone Copolymer), and DC-9045 (decamethylcyclopentasiloxane and Dimethicone Crosspolymer) were purchased from Dow Corning Corporation (Midland, MI). KSG-240 (dimethicone/PEG-10/15 crosspolymer and decamethylcyclopentasiloxane) and KF-995 were purchased from Shin-Etsu Chemical Corporation (Akron, OH). Pemulen TR-2 (Acrylates/C10-30 Alkyl Acrylate Crosspolymer), Ultrez 20 (Acrylates/C10-30 Alkyl Acrylate Crosspolymer), and UR-450 polyurethane were purchased from Lubrizol Corporation (Wickliffe, OH). Jeecide CAP-4 (Phenoxyethanol and Caprylyl Glycol) and Jeechem BUGL (butylene glycol) were purchased from JEEN International (Fairfield, NJ). Glycerin and propylene glycol were purchased from Ruger Chemical Co. (Linden, NJ). Sodium chloride and sodium hydroxide (10N) were purchased from Spectrum Chemical MFG Corp. (New

Brunswick, NJ). Nylon 10-I2 (Nylon 12 and Isopropyl Titanium Triisostearate) was purchased from Kobo Products (South Plainfield, NJ).

The lead RPB emulsion or Step 1 comprised 32% RPB 6 (see Table 1), 12% PMX-1184, 4% KSG-240, 0.1% FZ-2233, 50.32% water, 0.5% Pemulen TR-2, 0.5% Ultrez 20, 0.33% Jeecide CAP-4, and 0.25% 10N sodium hydroxide solution.

The Platinum Catalyst Delivery System or Step 2 comprised 10% DC9045, 4% KSG-240, 0.2% FZ-2233, 15.79% decamethylcyclopentasiloxane, 4.5% Nylon 10-I2, and 1.01% Karstedt platinum catalyst solution (2% platinum). The polyurethane and silicone wound dressing sheets were purchased from 3M (St. Paul, MN - Tegaderm™ Transparent Film Dressing 1626W) and Smith & Nephew (Andover, MA – Cica-Care® Silicone Gel Sheet). The bi-phasic remover was provided by Living Proof (Neotensil™ Remover, Cambridge, MA).

Formulation Procedures

Lead RPB Emulsion or Step 1:

In the main mixer, the lead RPB and emulsifiers were combined with the silicone phase diluents until a homogeneous mixture was visible. In a side mixer, the aqueous phase containing the polyacrylic acid hydrogel and preservatives were mixed until the aqueous dispersion appeared homogeneous. The aqueous phase was slowly introduced to the main mixer containing the silicone phase to form a white creamy emulsion. Finally, the emulsion was neutralized to target pH of 5.5 to 6.5.

Platinum Catalyst Delivery System or Step 2:

In the main mixer, the polysiloxane phase components and emulsifiers were mixed until the mixture was uniform in appearance. In a secondary mixer, the aqueous phase containing glycols, water and preservatives were mixed until the phase appeared homogeneous. The aqueous phase was slowly introduced to the silicone phase to form a clear emulsion. Nylon 10-I2 was slowly introduced to the main mixer and the emulsion was then homogenized. Finally, the Platinum catalyst was added to the emulsion and mixed until it was uniformly dispersed.

Mechanical Testing

Uniaxial tensile tests were performed with an Instron 3342 (Norwood, MA) based on ASTM D5083 methods. Briefly, a premix of the cure specimen ([Tetravinyltetramethylcyclotetrasiloxane: Karstedt platinum catalyst solution: RPB or the RPB emulsion], [0.50:0.50:99.00], w/w/w) was transferred into a dog bone mold (flat sheet type 0.5" wide) and cured for 24 hours. The cure specimen was then subjected to either 15 load-unload cycles at 15% tensile strain or 25 load-unload cycles at 100% tensile strain under room temperature to obtain a stress-strain plot or a hysteresis loop. Then, the cure specimen was subjected to a full tensile load until break where the tensile modulus and the fracture strain were evaluated from the stress-strain response.

Adhesion-in-peel tests were conducted using an Instron 3342 (Norwood, MA) based on ASTM C794 methods. Briefly, 0.75 g of a cure specimen premix ([Tetravinyltetramethylcyclotetrasiloxane: Karstedt platinum catalyst solution: RPB or the RPB emulsion], [0.50:0.50:99.00], w/w/w) was sandwiched in between two leather strips with a contact surface area of 1 inch by 2.5 inches and cured for 24 hours. The peel test procedure subjected one side of the cured leather strip to a 10 mm/sec extension until the leather strips completely separated. The adhesive force was averaged over the entire length of the cured location and normalized to the width of the sample.

Rheometer tests developed for measuring the cross-linking kinetics were conducted using the Bohlin CVO Rheometer (Malvern, UK) to implement a dynamic mechanical test based on ASTM D7750 standards. Briefly, a premix of the cure specimen ([Tetravinyltetramethylcyclotetrasiloxane: Karstedt platinum catalyst: RPB or the RPB emulsion], [0.67:0.33:99.00], w/w/w) was transferred to a 25-mm flat plate with a 250-micron gap size on the rheometer. The experiment was conducted at 70°C under the oscillatory mode with a 1-Hz frequency to obtain a plot of the storage modulus (G') over time. The cure time is defined as the transitional time from initial G' to the final G' and the cure rate is defined as the maximum slope of the plot of storage modulus (G') over time.

Pilot Human Studies

Study B: Normal volar forearm skin recoil study

The study protocol was approved by the Allendale IRB (Old Lyme, CT). Briefly, 6 women, ages 40 and older were enrolled in the study. Duplicate volar forearm skin sites of 3 cm by 3cm in area per panelist were assigned to three different treatments, XPL, Amlactin® Moisturizing Body Cream (Upsher Smith Laboratories, Morristown, NJ), and an untreated control site, following a predetermined randomized scheme. Measurements were taken at baseline, 24 hours after test article application and 30 minutes following test article removal. 0.08 mL of the lead RPB emulsion (Step 1) and 0.12 mL of the Platinum catalyst emulsion (Step 2) was applied to each designated site to create the XPL. AmLactin® (0.05 mL) was applied twice daily to the corresponding sites. The remover (1.5 mL) was applied to each of the 8 sites evaluated after the 24-hour measurement and left in contact with the XPL for at least 30 seconds to saturate and swell the film. The swollen film was then rolled off the skin using a cotton pad. Residual test article was removed with a dry tissue.

All suction cup measurements were taken following a 25-30 minute acclimation period in a controlled environment with the relative humidity maintained at less than 50% and temperature maintained at 19-22°C. A DermaLab® USB (Cortex Technology, Hadsund, Denmark) with a suction cup was used to evaluate skin elasticity following methods described in the literature[32,33]. Statistical analyses were conducted using a paired Student's t-test.

Skin conductance was measured in 24 volunteers (aged 25 to 55 years old) using a skin surface hygrometer (USB Dermalab with a flat-faced hydration probe, Cortex Technology, Hadsund, Denmark) for two test articles: petrolatum (Vaseline®, Unilever, Englewood Cliffs, NJ) and XPL. To enable probe contact with the skin during XPL wear, an annulus approximating the probe tip dimensions (1.4 cm^2 area) was created at the center of the 5 cm by 5 cm application site, where bare skin remained readily accessible to take the skin conductance measurements. All measurements were taken following a 25-30 minute acclimation period in a controlled environment with the relative humidity maintained at less than 50% and temperature maintained at 19-22°C. Measurements were taken at baseline and following test article application at 1 hour, 2 hours, 4 hours, and 6 hours. Statistical analyses were conducted using the Tukey's Post Hoc Test.

Study C: Dry skin study evaluating transepidermal water loss

The study protocol was approved by the Allendale IRB (Old Lyme, CT). A 9-point dryness grading scale was used to characterize the extent of skin dryness, where a score of 0 refers to no dryness and a score of 8 refers to severe, marked roughness. Healthy female volunteers, ages 40 and with visual dryness scores of 3, corresponding to moderately dry skin, or greater at each test site were included in the study.

Subjects were instructed to stop the use of all moisturizing products (soaps, lotions, sunscreens, insect repellents, etc.) on their legs during a 3-day pre-conditioning period prior to testing. Shaving was allowed up to 3 days prior to the start of the study and after the completion of the 24-hour measurements. Exercise or drinking of hot or caffeinated beverages within 2 hours prior to each instrument visit was discouraged as this could affect the measurements. Intensive, heavy exercise promoting excessive sweating was not permitted. The subjects were also instructed to wear shorts or pants that could be rolled above the knees to each visit.

Exclusion criteria included women with a skin condition other than dry skin at the test sites (such as psoriasis, eczema, and atopic dermatitis); subjects with marks (such as tattoos, and scars) at the test sites that might interfere with the visual grading, were also excluded from the study. Twenty-two subjects completed the entire study.

For each subject, two of the four test products were applied in duplicate to four of the five sites and the remaining site served as the non-treated control site. Test articles assigned to each site of the 5 outer calf test sites (3 sites on one leg and 2 sites on the other leg) were based on a predetermined rotation scheme.

A total of 0.15 mL of each XPL formulation was applied to cover the entire application site. Approximately 0.05 mL of petrolatum (Vaseline®, Unilever, Englewood Cliffs, NJ) and 0.05 mL of the commercial product (Crème De La Mer®, Estee Lauder Companies, New York City, NY) was applied to the corresponding designated test sites using a finger cot according to the randomization schedule. Expert graders were blinded to the application process.

Prior to baseline acclimation, subjects' test areas were cleansed with wet Kimwipes (Kimberly-Clark Corporation, Dallas, TX) and then patted dry with dry Kimwipes. The cleansing was as minimal as wiping twice with wet Kimwipes and subsequently "patting dry" by stroking twice

with dry Kimwipes. Five 5 cm by 5 cm skin test sites were then marked. Following the established methods described above, transepidermal water loss (TEWL) measurements were taken at baseline, two hours and twenty-four hours following test product application using a CyberDERM RG1 Evaporimeter (CyberDERM, Broomall, PA). Subjects reported for their 24-hour visit and the investigator determined the film integrity of the XPL treated sites. If the XPL was not minimally an 80% continuous film, the subject's participation in the study would end and Day 2 measurements would not be taken. For the TEWL values, a One-Way ANOVA was used to compare the net change from baseline at each time point. For all analyses, a two-tailed $p \leq 0.05$ was taken as the level of significance.

Study D: Double-blind, randomized, placebo-controlled, split face evaluation of XPL performance.

Optical coherence tomography (OCT, Michelson Vivosight OCT, Michelson Diagnostics, Raynham, MA) was utilized for non-invasive, *in-vivo*, real-time skin microscopy imaging to elucidate the skin hydration and topical mechanical shaping mechanism of the XPL technology. The clinical study was reviewed and approved by the Western Institutional Review Board (WIRB protocol number 20121506, Puyallup, Washington). Subjects between the ages of 40-75 with baseline lower lid severity scores of 3 or 4, based on a 0-4 photonumeric lower lid severity scale, were the primary inclusion criteria. A score of 0 corresponded to the absence of lower lid fat herniation, as visualized by the smooth facial contour observed from the lower lid to the cheek. A score of 4 described severe protrusion of the lower lid fat pad, where the lower lid fat pad extended beyond the midpoint of the distance defined by the lower lid to the cheek. For severe bags, the smooth facial contour is disrupted by the concavity of the boundary highlighting the bag. Twelve women were enrolled in the study.

Briefly, the XPL and a randomized placebo control were applied split face to the lower lid application sites following a predetermined randomization scheme. The placebo comprised the two steps of the XPL, or the vehicle, where the catalyst for the cross-linking reaction was absent from the Platinum catalyst delivery system. A Canfield Vectra 3-dimensional imaging system (Canfield Scientific, Fairfield, NJ) was used to capture the changes observed in the shape of the skin contours at baseline, 1 hour, and 4 hours following XPL application. OCT imaging and live

trained grader evaluations were also conducted with the evaluator blinded to the treatments at the three time points.

Metallic skin markers were applied to the under-eye area of each subject to enable consistent placement of the OCT probe at the same skin sites for each time point. For each under-eye area, three sites were consistently imaged at each of the three time points. These markers are identified by the arrows in the corresponding OCT images (Figure 6). These OCT images were analyzed to quantitatively assess the skin surface shaping effect of the XPL, using Image J (National Institutes of Health, Bethesda, MD).

The distance between the two epidermal markers was measured using a straight line (SLD). The epidermal surface length (ESL) was measured by tracing along the uneven epidermal surface in between the two markers. The surface irregularity (SI) values, described by the difference between the ESL and SLD (normalized by the ESL), were calculated at baseline, one hour, and four hours after XPL application. Values of SI that approach zero represent the ideal case of no surface roughness, as the ESL approaches the SLD.

The three sets of OCT image sections recorded for each skin site at baseline and at 4 hours for the vehicle and for the XPL were further analyzed to quantify the changes in the distribution of the pixel intensity. Sections of each image, comprising approximately 400 pixels in width and 40 pixels in thickness, immediately below the region identified as the stratum corneum, were selected by a blinded analyst. Due to area constraints placed by the sample geometries for a limited number of images, the area analyzed was reduced to remain contained within the epidermal layer. These image sections were then processed with Image J to calculate the average pixel intensity for each section selected. The Image J intensity scale is a 0 to 65,535 scale, corresponding to the dark and the lucent extremes of pixel intensity, respectively. After the average intensity was calculated for each site, the samples were un-blinded, and a student's t-test was implemented to determine the significance of the differences detected between the XPL and the vehicle groups.

Photography

Time lapse photographs were taken using three digital single lens reflex cameras (two Nikon D80 and one Nikon D300, Melville, NY), equipped with 17-70 mm macro lenses and circular polarizers, were positioned to simultaneously photograph the subject at three angles: 45 degree angles from the left and the right, and one at the center position. The subject was lit using 3 one-ft^2 - LED studio panel lights (Calumet, Chicago, IL), each providing 1400 LUX of 5600K lighting. Additional photographs were taken using a digital single lens reflex camera (Canon 5D Mark II, Canon U.S.A., Inc., Melville, NY) with an 85 mm lens (Sigma, Ronkonkoma, NY) and a strobe light unit (Alien Bees B800, Paul C. Buff, Nashville, TN) with an umbrella (Westcott, Maumee, OH) angled at approximately 45 degrees towards the subject.

Supplementary Information

Movie file: Figure3_ElasticityDemonstration.mov

Figure3_ElasticityDemonstration.mov

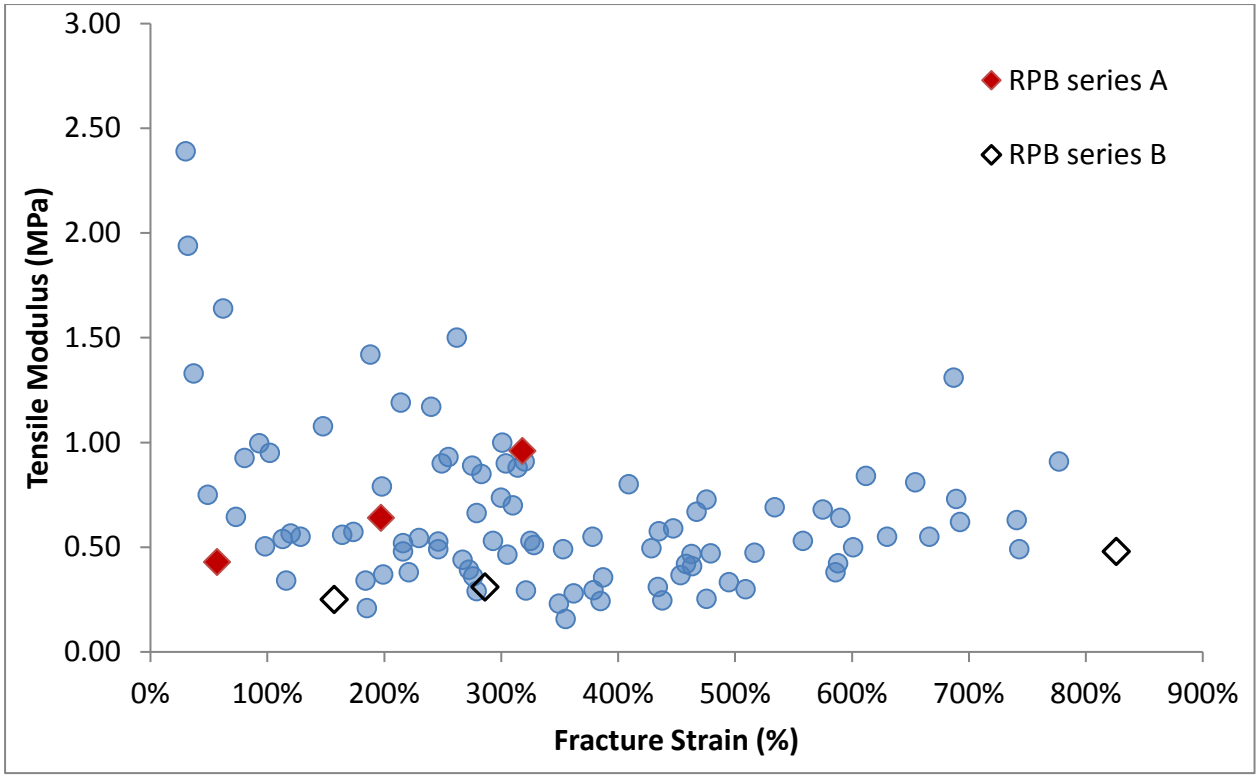

Figure 7: Broad utility of XPL materials platform space is depicted by the range of tensile moduli and the corresponding fracture strains achieved by modifying three materials design parameters: (1) the cross-linking density, (2) the molecular weight of functional polysiloxanes (vinyls and hydrides), and (3) the reinforcement particle loading. Subsets of lead RPB compositions are highlighted by the red diamonds and the open diamonds. The detailed mechanical properties of these compositions are described in Table 1.

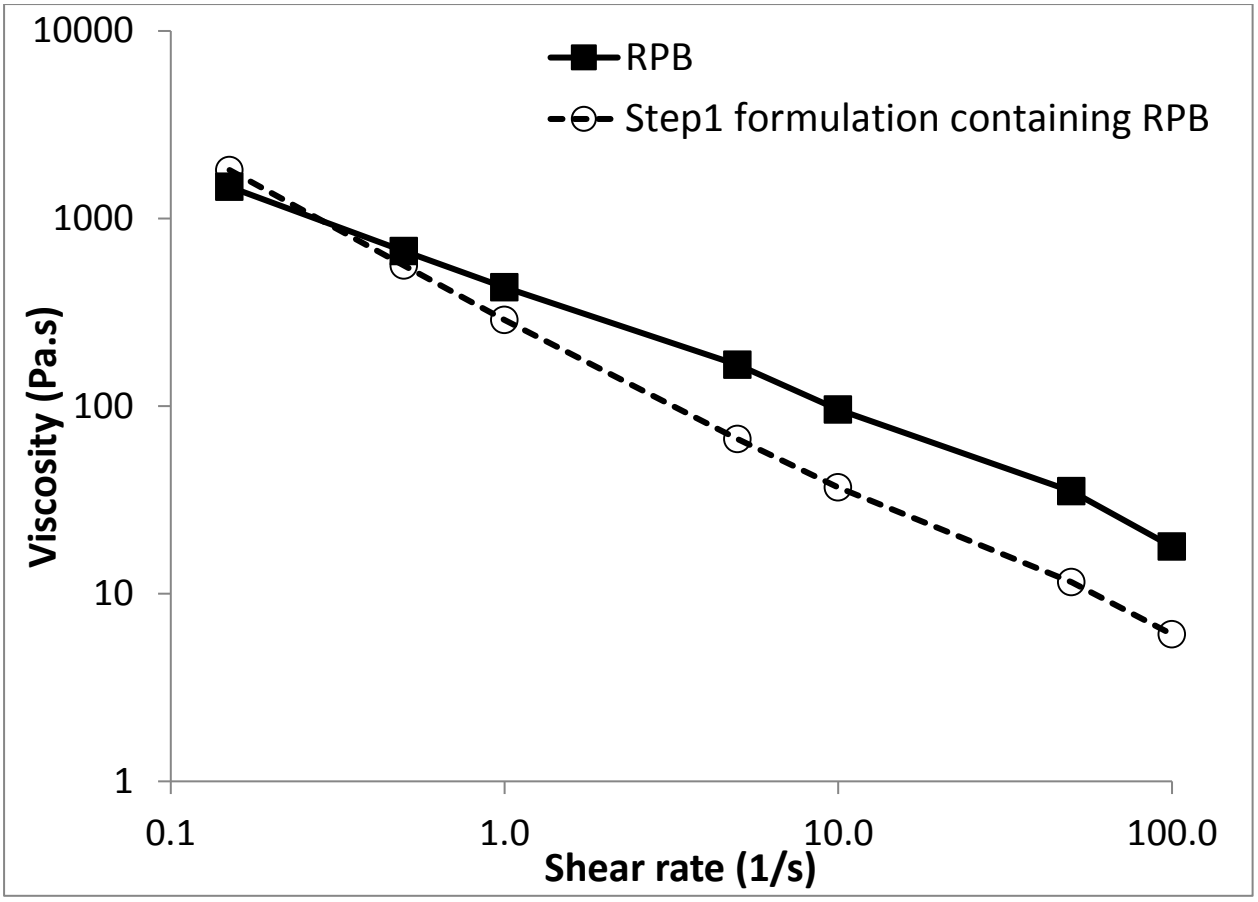

Figure 8: Shear thinning behavior of the Step 1 formulation containing RPB (open circle) versus that of the RPB alone (filled square).

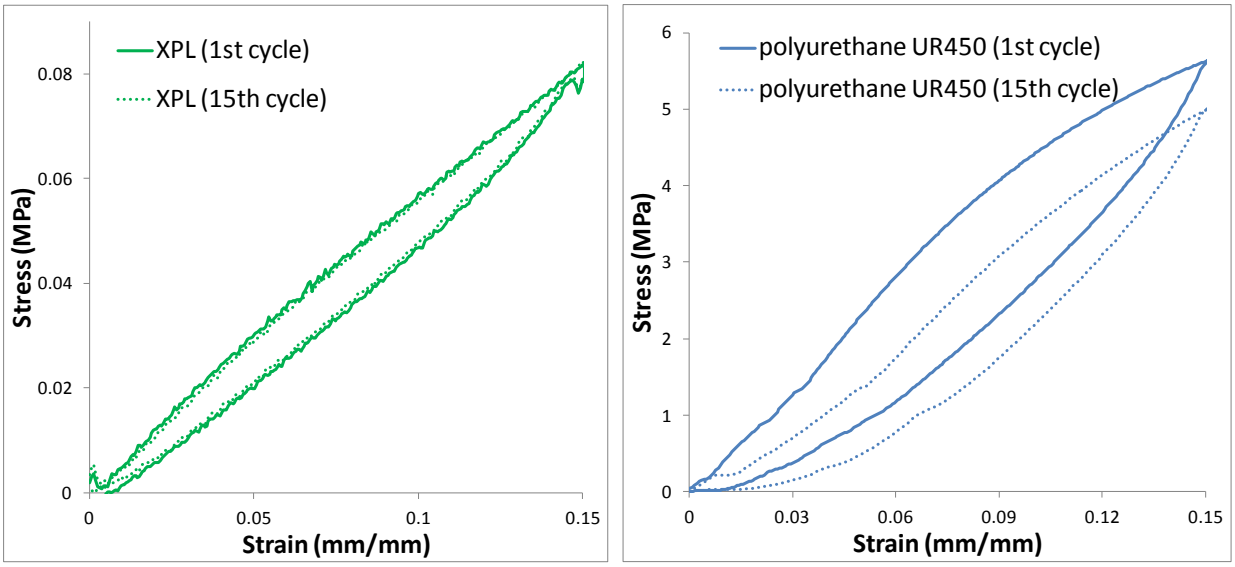

Figure 9: Side-by-side comparison of stress-strain hysteresis loops evaluating at 15% deformation over 15 load-unload cycles for the XPL (left figure) and a film formed by a commercial polyurethane Avalure™ UR450 dispersion (right figure). The hysteresis loop at the 15th cycle that drifts away from the hysteresis loop at the 1st cycle in the polyurethane UR450, in comparison to the XPL, indicated plastic deformation behaviour at 15% strain.

Reactive Polymer Blend (RPB) composition No.	Polysiloxane composition	Fumed Silica (wt%)	Leather Adhesion (N/mm)	Fracture Strain (%)	Tensile Modulus (MPa)	Plastic strain after tensile hysteresis (%)	Hysteresis loss energy density (kJ/m^3)
1	A	0%	4.71 (5.89)	57 (28)	0.43 (0.03)	0 (0)	0.035 (0.007)
2	A	15%	15.2 (3.69)	197 (14)	0.64 (0.02)	0.18 (0.15)	0.090 (0.017)
3	A	27%	58.0 (29.7)	318 (16)	0.96 (0.02)	0.45 (0.01)	0.443 (0.012)
4	B	0%	11.0 (1.53)	157 (11)	0.25 (0.02)	0.43 (0.01)	0.105 (0.007)
5	B	15%	70.0 (12.1)	286 (128)	0.31 (0.01)	0.76 (0.06)	0.240 (0.017)
6	B	27%	78.0 (2.74)	826 (120)	0.48 (0.03)	1.3 (0.26)	0.657 (0.017)

Table 1: RPB compositions and their associated material properties as a function of increasing fumed silica loading for two different polysiloxane compositions. Polysiloxane composition A contains 12.66% VS165K, 63.28% VS10K, and 24.06% XL-11. Polysiloxane composition B contains 13.57% VS165K, 58.04% VS10K, and 28.39% XL-11. Values are reported as the average of three samples. The standard deviations of the measurements are noted in parentheses. Six RPB compositions arising from two different lead polysiloxane compositions, RPB series A and B, each loaded at three different fumed silica concentrations (0%, 15%, and 27%) are highlighted by the red and the open diamonds in Figure 7. RPB (series B at 27% fumed silica concentration) is the lead composition evaluated. Polysiloxane composition A comprises a higher percentage of the short chained vinyl-terminated polysiloxane at 63.28% (versus 58.04% in RPB series B) and a lower cross-linker percentage at 24.06% (versus 28.30% for RPB series B). Close to a two-fold increase in modulus was measured for the RPB series A compared to RPB series B at each fumed silica loading (0.43, 0.64, and 0.96 MPa compared to 0.25, 0.31, and 0.48 MPa, for 0%, 15% and 27% fumed silica loading, for RPB series A and for RPB series B, respectively). Moreover, incremental increases in the fumed silica loading increased the leather adhesion, fracture strain, and tensile modulus within each polysiloxane blend composition. For each of these compositions, the plastic strain after cyclic hysteresis testing remained close to only 1% and the dissipative (hysteresis loss) energy density calculated from the area delineated by the hysteresis loop was less than 0.7 kJ/m^3. Lead RPB series B (No.6) at high silica loading was selected as the material basis for the formulation development because of the superior leather adhesive strength (78 N/mm) and elongation properties (fracture strain over 800%), compared to the other RPB compositions listed.

Time point	XPL	Vehicle
baseline	31477[*] (3708)	30878[**] (3821)
4 hours	25888[*,#] (3207)	28774[**,#] (3535)

Table 2: Skin hydration measurements based on calculations of average epidermal pixel intensity of OCT image sections for XPL and vehicle exposed skin sites. The average pixel intensities for the XPL and the vehicle treated sites are shown for the total of 36 OCT image sections that were analyzed per treatment group. Dark pixels, or lower intensity values, reflect regions of greater hydration, based on the OCT imaging technique. The differences measured for the XPL group and for the vehicle group at four hours compared to their baseline intensities were significant (*$p<0.00001$, **$p<0.05$, respectively), translating to average pixel intensity decreases of 18% and 7%. The XPL sections showed a significantly lower average pixel intensity compared to the vehicle ($^{\#}p<0.001$). The standard deviation of the mean is reported in parentheses. Statistical significance determined using paired Student's t-tests.